

MASSACHUSETTS INSTITUTE OF TECHNOLOGY
DEPARTMENT OF MECHANICAL ENGINEERING
CAMBRIDGE, MA 02139 USA

Room: 3-469a
Tel: (617) 253-2144
FAX: (617) 258-7881
E-mail: dubowsky@mit.edu
May 29, 1999

NASA INSTITUTE FOR ADVANCED CONCEPTS

To Whom It May Concern,

Enclosed is our final report for our Phase II NIAC contract number NAS5-9801.

Organization and Department:	Massachusetts Institute of Technology Department of Mechanical Engineering 77 Massachusetts Avenue Cambridge, MA 02139 USA
Project Title:	Self-Transforming Robotic Planetary Explorers
Type of Organization:	Educational
Principal Investigator:	Professor Steven Dubowsky, Room 3-469a Department of Mechanical Engineering Massachusetts Institute of Technology 77 Massachusetts Avenue Cambridge, MA 02139 Tel: (617) 253-2144 FAX: (617) 258-7881 E-mail: dubowsky@mit.edu
Business Contact:	Kristin Ryan, Administrator Office of Sponsored Programs, Room E-19-750 Massachusetts Institute of Technology 77 Massachusetts Avenue Cambridge, MA 02139 Tel: (617) 253-1696 FAX: (617) 253-4734 E-mail: kry@mit.edu
Call for Proposal:	NIAC 99-01 -- 1999 Phase II Advanced Aeronautical/Space Concept Study
Start Date:	July 1, 1999
End Date:	February 28, 2002



Steven Dubowsky, Professor

I. Introduction

The exploration and development of the planets and moons of the solar system in the next 10 to 40 years are stated goals of NASA and the international space science community. Robots will be required for missions to explore these bodies and in some cases build out-posts. A robot for a planetary exploration mission may need to traverse varying terrain obstacles, climb steep cliff faces, cross wide ravines and canyons, and assemble structures. Mars terrain is rough, with enormous canyons and mountains almost three times higher than Mt. Everest. We have proposed and studied the concept of self-transforming robotic planetary explorers (STX) to meet the needs of these future missions. Detailed system simulations have been performed to evaluate the feasibility of our concept. Prototype components have been built and experiments have been successfully conducted for the proposed concepts.

A self-transforming robotic system would be able to change its configuration to overcome a wide range of physical obstacles and perform a wide range of tasks. It would enable robot scouts to lead the way, exploring, mapping and constructing facilities. A new design paradigm – binary space robotics has been explored to achieve such a system. It includes a 21-DOF orbital camera articulated mount, a 30-DOF rovers capable of camera manipulation, rock coring, robot mating (to assemble themselves into larger organisms), and a six legged 126-DOF walking robot capable of walking in rough terrain (see Figure 1). Experimental prototype binary devices and elements have also been designed and constructed. The first generation Binary Robotic Articulated Intelligent Device (BRAID) is an all-plastic device, where only the wires are metal. The second generation BRAID II uses integrated bi-stable latching and polymer cross-flexures. The third generation BRAID III uses Electrostrictive Polymer Artificial Muscles (EPAM) as actuators.

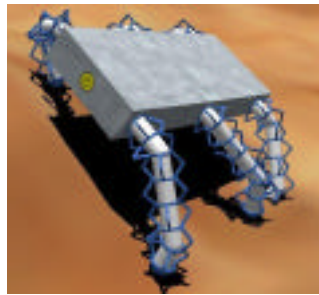


Figure 1: A six legged 126-DOF walking robot

The next step would be hyper-redundant binary devices with many degrees of freedom implementing distributed flexibility to achieve large motions. Ultimately, one would like to send bags of plastic to Mars and have them assemble themselves into robots that will achieve objectives of the future.

II. Key Technology Developed

The self-transforming robotic system presents a number of important technical challenges, such as in the areas of sensor technologies, communications and artificial intelligence. Our studies have focused on the problems associated with the design of the physical system and its control that are relevant to the needs of NASA in the 10 to 40 year period.

a) System-Level Planning, Analysis and Simulation

Binary robotic systems consist of a large number of binary actuators, as opposed to a small number of continuous ones, many control and planning issues are fundamentally different from those of conventional robotic systems. Analysis and simulation have been performed to examine the feasibility of controlling and planning binary robotic systems in representative exploratory tasks. Appropriate planning algorithms on kinematics, trajectory following, locomotion planning and coordination have been developed. These algorithms can be imported directly into physical implementations without major revision. In summary, we have demonstrated that a self-transforming robotic system of a large number of binary states (10^3 to 10^4) can deliver the changing topology necessary for truly effective planetary robots.

b) Actuator Technology and Hardware Demonstrations

One of the main challenges to implement the concept of STX is to have an appropriate actuator that is compact, simple, lightweight and can be operated easily in a binary manner. Two types of such binary actuators have been successfully designed and built. One is a SMA-based antagonistic actuator with internal detents and flexure beams. Figure 2 shows a prototype of this SMA actuator. The other is an Electrostrictive Polymer Artificial Muscle (EPAM) actuator with many advantages such as high strain, low power consumption, high flexibility and low weight. Figure 3 shows a prototype of this EPAM actuator and its application to a module-based re-configurable structure.



Figure 2: The prototype of a SMA-based antagonistic actuator

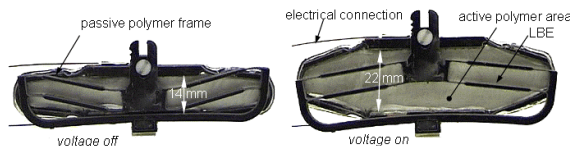


Figure 3: An EPAM actuator and its application to BRAID structure

The work that has been done provides an excellent foundation for developing transformable robotic systems for planetary exploration purposes. Given time and research, each of the elements of the STX concept will reach a sufficient state of development to allow the full vision to be realized.

III. Publications and Student Thesis

The published papers that have resulted from this work below are listed below. These are being provided to NIAC as pdf files.

a) Publications

Hafez, M., Lichter, M., Dubowsky, S., “Optimized Binary Modular Reconfigurable Robotic Devices,” submitted, *IEEE/ASME Journal of Mechatronics*, 2002.

Hafez, M., Lichter, M., Dubowsky, S., “Optimized Binary Modular Reconfigurable Robotic Devices,” *Proceedings of 2002 IEEE International Conference on Robotics and Automation*, Washington D.C, May, 2002.

Lichter, M., Sujan, V. Dubowsky, S., “Computational Issues in the Planning and Kinematics of Binary Robotics,” *Proceedings of 2002 IEEE International Conference on Robotics and Automation*, Washington D.C, May, 2002.

Lichter, M.D., V.A. Sujan, and S. Dubowsky, “Experimental Demonstrations of a New Design Paradigm in Space Robotics,” *Proceedings of the Seventh International Symposium on Experimental Robotics*, Honolulu, Hawaii, December 2000.

Sujan, V., Dubowsky, S., “Visually Built Task Models for Robot Teams in Unstructured Environments,” *Proceedings of 2002 IEEE International Conference on Robotics and Automation*, Washington D.C, May, 2002.

Sujan, V.A., M.D. Lichter, and S. Dubowsky, “Lightweight Hyper-redundant Binary Elements for Planetary Exploration Robots,” *Proceedings of the 2001 IEEE/ASME International Conference on Advanced Intelligent Mechatronics*, Como, Italy, July 2001.

Wingert A., Lichter M., Dubowsky S., Hafez M., “Hyper-Redundant Robot Manipulators Actuated by Optimized Binary Dielectric Polymers”, to be published in Smart Structures and Materials 2002: Electroactive Polymer Actuators and Devices, *Proceedings of SPIE Optical Engineering Journal*, Vol. 4695, 2002.

Wingert, A., Lichter, M., Dubowsky, S., “On the Kinematics of Parallel Mechanisms with Bi-Stable Polymer Actuators,” *Proceedings of 8th International Symposium On Advances in Robot Kinematics*, Caldes de Malavella, Spain, June, 2002.

b) Thesis

The following student theses have resulted from this research.

Andrews, Kate, “Elastic Elements with Embedded Actuation and Sensing for Use In Self-Transforming Robotic Planetary Explorers,” Master Thesis, Department of Mechanical Engineering, MIT, 2000

Fontaine, Ebraheem, “A Laboratory Demonstration of a Parallel Robotic Mechanism with Integrated EPAM Actuators,” Bachelor Thesis, Department of Mechanical Engineering, MIT, 2002.

Lichter, Matt, “Concept Development for Lightweight Binary-Actuated Robotic Devices, with Application to Space Systems,” Master Thesis, Department of Mechanical Engineering, MIT, 2001

Oropeza, Guillermo, “The Design of Lightweight Deployable Structures for Space Applications,” Bachelor Thesis, Department of Mechanical Engineering, MIT, 1999.

Rapp, Lani, “Design of a Mechanism to Amplify the Motion of Shape Memory Alloys,” Bachelor Thesis, Department of Mechanical Engineering, MIT, 2001

Weiss, Peter, “Development and Optimization of Electrostrictive Polymer Artificial Muscles Actuators with Large Expansions and High Forces,” Diplome D'Ingenieurs, Ecole Polytechnique Femenine (EPF), Paris, France, 2001.

Wingert, Andreas, “Development of a Polymer-Actuated Binary Manipulators,” Master Thesis, Department of Mechanical Engineering, MIT, 2002.

Optimized Binary Modular Reconfigurable Robotic Devices

Moustapha Hafez Matthew D. Lichter Steven Dubowsky
Department of Mechanical Engineering, Massachusetts Institute of Technology
Cambridge, MA 02139 USA, Email: hafez/lichter/dubowsky@mit.edu

Abstract

Binary robotic devices with large numbers of degrees of freedom have been proposed by a number of researchers. However, experimental implementations of these concepts have been built with conventional components. These physical systems are heavy, complex, and far from being practical devices. In this paper, a lightweight, compliant mechanism driven by optimized magnet-coil actuators is proposed and developed as an element for modular hyper-redundant robotic systems. Such elements could be used in a number of applications and would replace conventional, complex, and heavy components. The device has a parallel kinematics structure. Its binary actuation simplifies its control architecture. Analytical and experimental results for a practical prototype system are presented.

1. Introduction

Challenging applications are being proposed for robotic systems such as robots for surgery, service in the home, and space exploration [1]. Researchers have proposed robotic systems based on binary movements [2-5]. These devices, which can be called digital mechanisms, are able to perform precise, discrete motions without need for sensing, complex electronics, or feedback control. Traditional mechanisms have a small number of continuous degrees of freedom (DOF). A digital mechanism approximates this motion by using a large number of binary DOF. The larger the number of DOF, the smaller the position and orientation error [6,7]. Recent studies have considered the kinematic motion of these devices in more depth [8]. However, most experimental implementations of the concept have been done with conventional components using elements such as bearings and gears. Since a large number of DOF are required, they are heavy, expensive and not practical. Therefore, new design paradigms are required for such systems.

An optimized binary modular reconfigurable device is proposed in this paper. It has potential applications in the biomedical field such as camera or light positioning for surgeon assistance. Moreover, such elements could be used as key components for self-transforming robots for planetary exploration [6,7,9,10]. The overall design is based on the assembly of modular parallel platforms. This allows the device to reconfigure itself to achieve

mechanisms of different characteristics. A magnet-coil actuator is used to drive the structure. Based on electromagnetic theory, an analytical model of the actuator is introduced to optimize its geometric parameters and maximize its efficiency. The discrete nature of the mechanism is ensured by the use of bistable mechanisms (briefly discussed in this paper). Deployable structures that are stable at a discrete set of configurations could also be used [11]. The binary deployable structures discussed in this paper are given the name Binary Robotic Articulated Integrated Devices (BRAID). A BRAID (see Figure 1) is a network of flexible and rigid members with binary embedded actuators. It is a lightweight, simple, and robust mechanism that is fault-tolerant. The BRAID is composed of a large number of parallel stages, which have three DOF each (two rotations and one translation) mounted in a serial configuration. Each single stage can achieve $2^3 = 8$ possible configurations. The end stage has five DOF (two rotations and three translations).

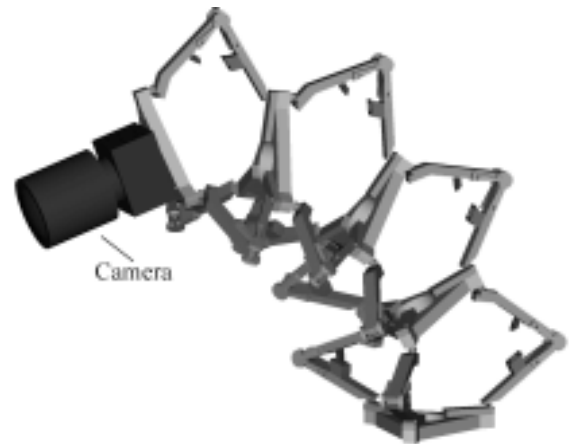


Figure 1 – The BRAID has five DOF which allows for precise camera placement.

The BRAID concept was based on polymer actuators that have yet to realize their projected performance [12]. A first BRAID version was developed based on shape memory alloy (SMA) actuators [10]. However, for the BRAID such actuators are slow, inefficient, and have poor thermal properties as they dissipate a lot of heat and can be triggered by changing environmental conditions. The second generation BRAID presented here has electromagnetic actuators. This design is intended to demonstrate that it is feasible to construct practical binary devices. This paper addresses design issues such as

flexure design and bistable mechanisms and discusses the detailed actuator modeling and optimization. Simulations [7] and experimental results suggest that practical binary devices with large number of DOF can be achieved with current technology.

2. BRAID design

BRAID structures are made largely of polymer materials (plastics) to make them lightweight. Figure 2 shows an exploded view of a single stage. The three legs each have two one-DOF flexural bearings, which can rotate by $\pm 25^\circ$ and $\pm 17^\circ$ respectively. This eliminates the need for heavy conventional bearings with their friction, backlash, and added weight. The system also decreases the demands on the actuators. One cone-ball sliding bearing with three rotational DOF is used for each leg. This sliding bearing satisfies the large angles of tilt up to $\pm 60^\circ$, while keeping a high structural stiffness. This is difficult to achieve with flexural bearings. The stages are mounted on each other using magnetic preload forces between permanent magnets and steel parts. This magnetic connection enables a modular design, which is of prime importance for reconfigurability. The structure is driven by electromagnetic actuators composed of curved magnets and coils to minimize the air gap between the actuator components. Finally, bistable mechanisms are integrated in the design to enforce the binary discrete motion. These also eliminate the need to power the device to hold it in position.

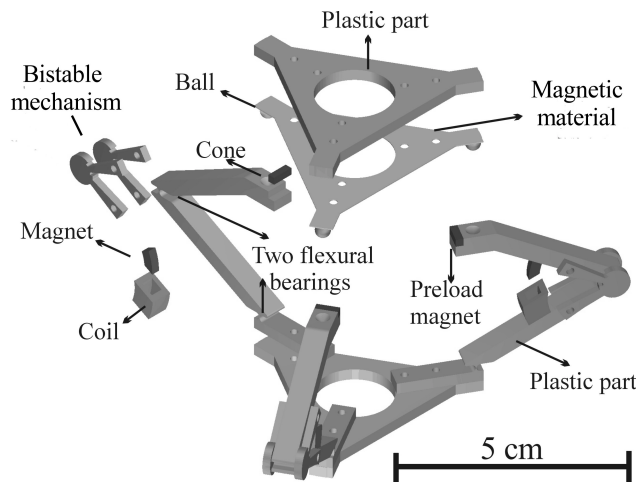


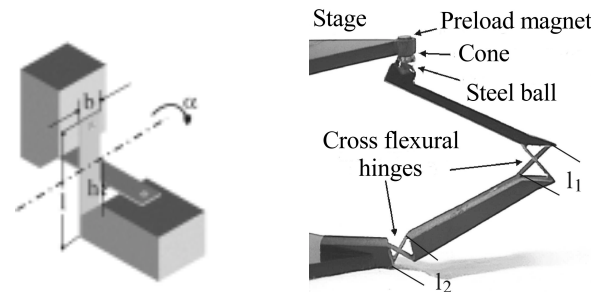
Figure 2 - Exploded view of a single stage.

The material selected for the BRAID structure, which incorporates both flexural and sliding bearings, is Delrin® 100 (PolyOxyMethylene with 20% Teflon). Delrin® has high tensile strength, impact resistance, stiffness, and fatigue endurance. These properties make it a good choice for flexural hinges. Delrin® has excellent wear and friction behavior due to its natural lubricity. Such

properties lead to highly efficient sliding bearings. Delrin® is also easily machinable using water-jet cutting technology and traditional machining processes. The key elements of the BRAID, which are discussed in detail below, are its bearings, actuators, and bistable mechanisms.

2.1 Design of compliant bearings

Flexural bearings are wear-free and their motions are smooth and continuous. The accuracy of a flexural bearing depends on how well the bearing is assembled and machined. They have high repeatability and resolution. However, they have some disadvantages. The stiffness of such bearings is inversely proportional to the range of motion. They are sensitive to thermal variations especially when made from polymers. They cannot tolerate large loads and are susceptible to buckling. Finally, a flexible connection might result in vibration problems in some high-speed applications. The flexible pivot configuration chosen for the BRAID is based on cross-flexural hinges (see Figure 3a). It consists of a pair of crossed plastic leaf springs of uniform length (l), width (b), and thickness (h). Compared to other types of flexural bearings, cross-flexural hinges greatly improve fatigue life, range of motion, and out-of-plane stiffness.



(a) cross-flexural hinge (b) BRAID stage
Figure 3 – Flexural bearings.

Angular stiffness

For small angular deflections of the bearing (α), it is convenient to assume that the springs deform in a circular arc shape. In this case the angular stiffness (K_α) of the cross-springs is twice the stiffness of a single leaf spring in pure rotation.

$$K_\alpha = \frac{2EI}{l} \quad \text{where} \quad I = \frac{bh^3}{12} \quad (1)$$

(I) is the moment of inertia, and (E) the Young's modulus of elasticity. For larger angular deflections such as required for the BRAID ($\alpha = \pm 25^\circ$), the strip does not deform exactly in a circular arc and its stiffness is higher. For such angular deflections, stiffness increases by less than 10% [13,14].

Angular deflection limits

If the springs are assumed to deform in the shape of a circular arc, then the allowed deflection (α_{all}) of the cross-spring hinge is equal to the deflection of a single leaf spring and is given by:

$$\alpha_{all} = \frac{2\sigma_{all}l}{Eh} \quad (2)$$

For larger angles, the allowable stresses in the springs (σ_{all}) increase due to a non-circular arc deformation. For an angular deflection of 45° , the stress is 30% greater for the same deflections given by equation (2) [14].

The Delrin® has a 10^7 cycles fatigue stress (σ_{all}) of 30 MPa and its Young's modulus is 2600 MPa [15]. Using these values and a safety factor, the leaf springs in the BRAID (see Figure 3b) have the following dimensions of $l_1 = 10.7$ mm (0.424"), $l_2 = 7.2$ mm (0.283"), $b = 3.175$ mm (0.125"), and $h = 0.51$ mm (0.02") to achieve 10^7 cycles of $\pm 25^\circ$ and $\pm 17^\circ$ for l_1 and l_2 respectively. A life of 10^7 cycles is quite adequate for most robotic applications.

2.2 BRAID Sliding bearing design

Because sliding contact bearings often distribute loads over a large area, contact stresses and space requirements are often low while stiffness and damping are usually high. A spherical bearing, which is composed of a ball that slides in a cone, is appropriate for the kinematics of the BRAID structure as it provides three rotational DOF. The materials for this bearing were selected to give minimum wear and friction. Polymers in contact with a hard material with very low surface roughness meet this objective. The result is low adhesive interaction at the contact points, which leads to low friction, minimal stick-slip effect, and relatively low wear. A cone made of Delrin® and a ruby ball appears to be almost an ideal combination [17]. However to preload the joint by using a magnet beneath the cone, a corrosion resistant magnetic steel ball is used. This bearing has a life that approaches 10^7 cycles. In order to ensure an accurate tilt, almost no wear is allowed on the ball and just slight wear on the cone. Comprehensive wear and friction analyses for this type of sliding bearing have been done previously [16,17].

3. Electromagnetic actuator design

Electromagnetic actuators (also called voice coils) are frequently used in high performance and high precision applications such as disk drive head positioning. They were selected for the BRAID because the main actuator design criteria are the deliverable force, the power

dissipation, and the total volume and mass of the actuator. The choice of magnet and coil geometry with a rectangular cross-section was made mainly on the available space in the BRAID structure and on the manufacturing technologies offered. Closed-form expressions have been derived for the levitation forces between two circular magnetic discs and two non-coaxial circular coils [18,19]. While an optimized circular magnet-coil force actuator and its application to precision elastic mechanisms has been presented [20], almost no literature is available for coils with rectangular cross-sections. Based on the laws of magnetostatics and the magnetic vector potential (\vec{A}), an analytical model was developed in this study to determine the force between the curved magnets and coils with a rectangular cross-section and is briefly presented below.

An analytical model of a magnet-coil actuator with rectangular cross-section

The X-component of the magnetic vector potential (A_x) in a wire segment of length (L_1) (see Figure 4a) going in the X-direction, with its middle point at the origin and in which is flowing a current (I_1) is given by [21]:

$$A_x = \int_{-L_1/2}^{L_1/2} \frac{\mu_o}{4\pi} \cdot \frac{I_1}{\sqrt{(x_1 - x)^2 + y^2 + z^2}} dx_1 \quad (3)$$

The magnetic field (\vec{B}) created by this current is derived from $\vec{B} = \vec{\nabla} \times \vec{A} = \text{curl} \vec{A}$. In the case of a straight wire positioned along the X-axis, the X-component of the magnetic field (\vec{B}) is zero and the two other components are given in the following equations:

$$B_x = 0, \quad B_y = \frac{\partial A_x}{\partial z}, \quad B_z = -\frac{\partial A_x}{\partial y} \quad (4)$$

For two wire parallel segments (see Figure 4a), one of length (L_1) and with a current (I_1) and the other wire of length (L_2) with a current (I_2), there is an attractive or repelling force between them. The direction of the force depends on the currents' directions. An attractive force is created if the two currents flow in the same direction. The Y and Z components of the force acting on wire 2 due to the current flowing in wire 1 can be determined from the general equation of Lorentz force:

$$\vec{F} = \oint Id\vec{l} \times \vec{B} \quad (5)$$

where ($d\vec{l}$) is an element along the length of the conductor. The (F_y) and (F_z) are expressed as follows:

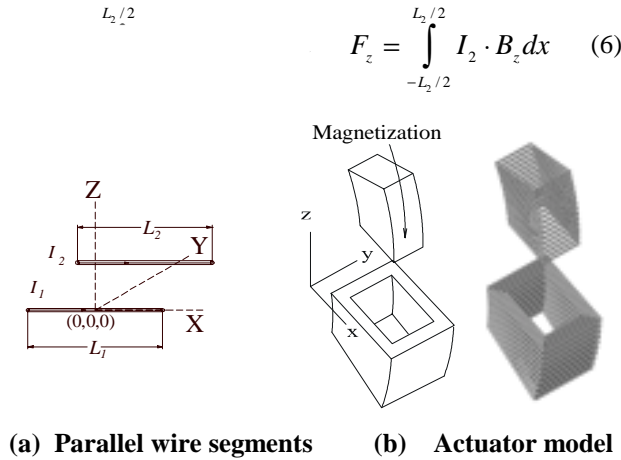


Figure 4 – Electromagnetic actuator.

These formulas can be applied to calculate the resulting force between a magnet and a coil. In fact, it is possible to represent a permanent magnet by a coil, which has one single layer of a conducting material with a certain number of turns. The curved axis of the coil corresponds to the magnetization direction of the permanent magnet. Therefore, the following relation applies:

$$N \cdot I = \frac{B_r}{\mu_o} \cdot h_{mag} \quad (7)$$

where (N) is the number of turns, (I) the current flowing in the coil, (B_r) the remanence of the magnet, and (h_{mag}) is the height along magnetization. This equation is valid in the case where the BH-curve is a straight line in the second quadrant. On the other hand, when the material has a non-linear behavior, the right hand side term of equation (7) should be divided by the relative recoil permeability (μ_r). The actuator can be represented by an equivalent analytical model (see Figure 4b). The two components of the force between each single wire and all the other parallel wires in both the x and y directions are calculated from equations (6). In the case of full symmetry, which means that the two coils are coaxial, the forces acting in the y direction between two parallel wires cancel. The sum of forces along the z-axis (F_{act}) gives the force generated by the actuator.

$$F_{act} = \sum F_z \quad (8)$$

Because of the BRAID binary action, actuators are not judged on linearity, accuracy, or resolution but on the force delivered. Figure 5 shows a plot of the calculated force delivered by the linear actuator as a function of the distance between the center of gravity of both the magnet and the coil (D). The Nd-Fe-B magnet dimension is 10 x 6 x 6 mm³ and the coil is 15 x 15 x 14 mm³ with a

thickness of 4.2 mm. The number of turns (N) is 250, and a peak current of 3A is used.

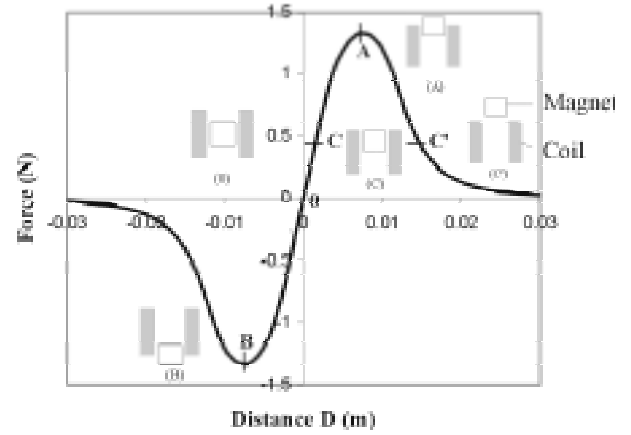
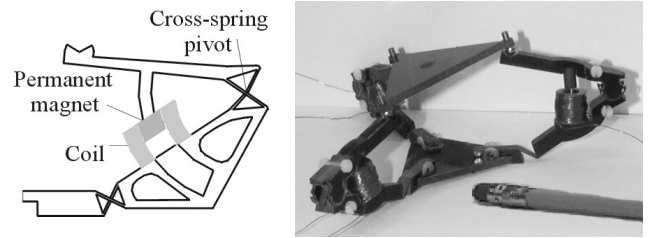


Figure 5 - The calculated magnetic force.

The position of the magnet with respect to the coil is very important as the force varies significantly from one position to another. It should be noted that when the two centers of gravity coincide (D = 0), the force delivered by the actuator is zero. The force increases to a maximum value when the magnet is partially in and partially out (positions A and B). The force then decreases exponentially as the two components move apart.

In the BRAID actuators act in parallel with bistable mechanisms that hold the structure in either of the two desired positions even when the power is off. Power to the actuators is only required to move from one state to another. Using low-duty-cycle impulses in the millisecond range as input signals to the actuator allows the use of peak currents that are relatively high (several amperes) while keeping power dissipation in the coil at an admissible level.



(a) Side view (b) Single Braid stage

Figure 6 - Prototype with a limited angle of rotation.

If just one side of the coil is used (see Figure 6), it is quite difficult to get an efficient binary actuator although it is possible to achieve moderate deflections. The two binary states will lie on each side of the peak shown in Figure 5 as the two points indicated C and C'. A more efficient actuation method is to use both ends of the coil where the

magnetic field is at maximum. This is achieved with two magnets with inverted polarities (see Figure 7).

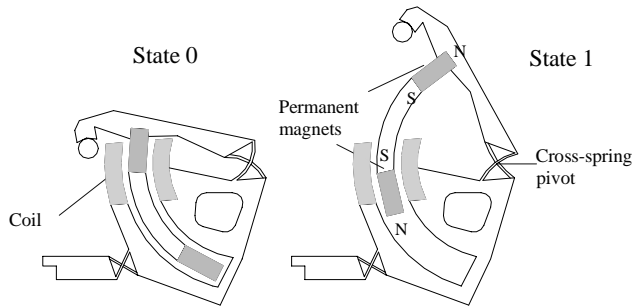


Figure 7 – Working principle of a binary actuator based on two magnets of inverted polarities.

The contributions of the two magnets add. The advantage of such a design is that the amplitude of the stroke can be increased without significantly increasing inertia of the mobile part. The force remains high over the actuator stroke.

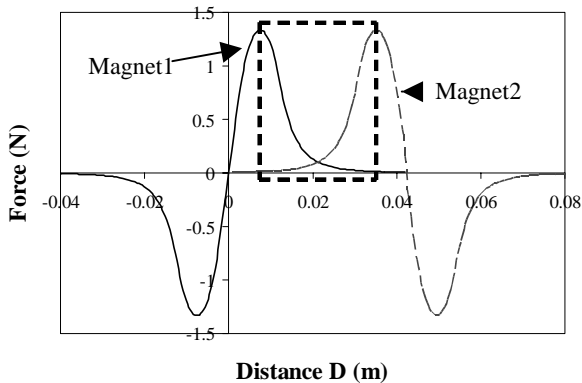


Figure 8 - Calculated magnetic force for a dual push-pull actuator as a function of the distance (D).

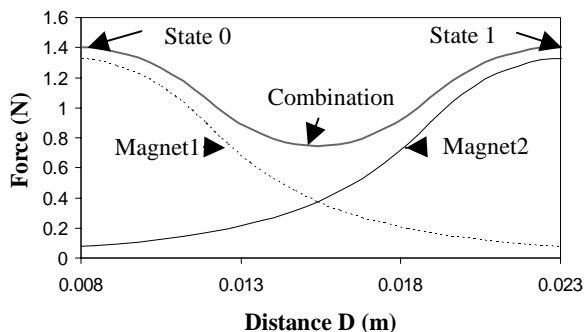


Figure 9 – Combined force delivered by the actuator. Figure 8 shows the calculated force from the model as a function of the distance between the different components (magnet1, magnet2) relative to the coil (same dimension as previously indicated). The second curve indicated in Figure 9 is a close-up of the area of interest. The two magnets' curves are added and the resulting force of the

actuator has roughly a sinusoidal shape. The maximum points on the curve are chosen to be at the two states of the binary actuator. It should be noted that the force is relatively high over the entire stroke.

4. Bistable mechanisms design

Bistable mechanisms (devices with two stable equilibrium states within their range of motion) are commonly used as switches, closures, or hinges. They provide accurate and repeatable motion. They require no power to remain in equilibrium state.

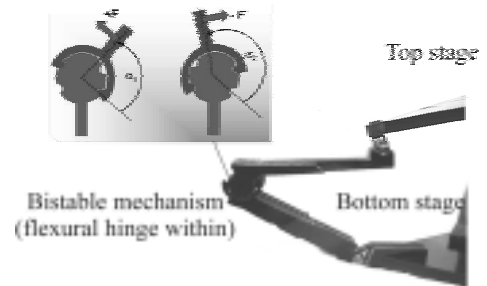


Figure 10 – Bistable detent that locks each leg of the BRAID in two discrete positions.

Figure 10 shows a possible design that can easily be implemented in the BRAID. The accuracy of the motion is achieved through the flexural hinge, which is located behind the bistable mechanism. The bistable mechanism then locks the structure in its two discrete positions using detents. An alternative for bistability can be achieved with the snap-through of a buckled beam to maintain two distinct states (see Figure 11). Full analysis of these bistable mechanisms is beyond the scope of this paper.

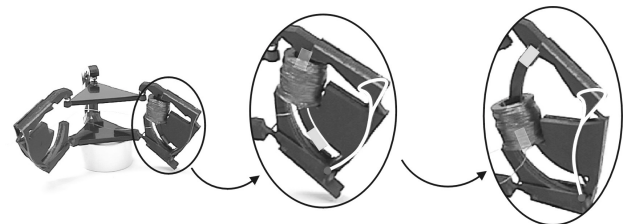


Figure 11 – Bistable compliant mechanism.

Figure 12 shows a two-stage electromagnetically actuated BRAID prototype in various configurations. The end stage has five DOF. When stowed, the structure is 7 cm tall; when deployed it is 11 cm tall, which is about a 60% increase. The mass of each single stage is less than 65g. The two-stage structure is able to lift a 200g mass positioned on the upper platform.

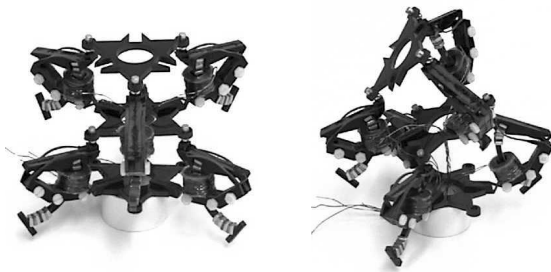


Figure 12 - Two-stage electromagnetically actuated BRAID prototype in various configurations.

5. Conclusion and perspectives

The Binary Robotic Articulated Integrated Device (BRAID) presented in this paper is a concept module for robotic systems that are capable of accomplishing tasks of substantial complexity, with flexibility and robustness. The electromagnetic actuator proposed provides considerable force to drive the structure and provides large deflections that lead to a large workspace of the manipulator. The bistable mechanisms introduced in this paper lock the structure into discrete states to conserve power and provide high accuracy and repeatability. For a more efficient design that allows a larger number of stages, each module will be designed according to the mass it is required to displace. Thus the stage located at the base will be larger than the end stage used for tool manipulation, since it will require larger and more powerful actuators. The BRAID silhouette will have a conical shape rather than a cylindrical shape, which will also increase the resolution of the manipulator. Currently applications for BRAID devices are being studied which include assistance devices for operating rooms and camera positioning mechanisms for mobile robots.

Acknowledgements

The authors acknowledge the NASA Institute for Advanced Concepts (NIAC) for supporting this research. Also, the important contributions of Ebraheem Fontaine, Vivek Sujan, and Andreas Wingert in the fabrication and design analysis are acknowledged.

References

- [1] Huntsberger, T.L., Rodriguez G., and Schenker P.S. "Robotics: Challenges for Robotic and Human Mars Exploration" Proceedings of ROBOTICS2000, Albuquerque, NM, Mars 2000.
- [2] Anderson V.C., and Horn R.C., "Tensor Arm Manipulator Design" ASME paper, 67-DE-57, 1967.
- [3] Roth B., Rastegar J., Scheinman V., "On the Design of Computer Controlled Manipulators" First CISM-IFTMM Symposium on Theory and Practice of Robots and Manipulators, pp 93-113, 1973.
- [4] Chirikjian, G.S. "A Binary Paradigm for Robotic Manipulators" Proc. IEEE International Conference on Robotics and Automation, pp. 3063-3069, San Diego, California, USA. May 8-13, 1994.
- [5] Chirikjian, G.S. and Ebert-Uphoff, I. "Discretely Actuated Manipulator Workspace Generation Using Numerical Convolution on the Euclidean Group" Proceedings of the 1998 IEEE, International Conference on Robotics and Automation, Leuven, Belgium. May 16-21 1998.
- [6] Lichter, M.D. Sujan, V.A., and Dubowsky, S., "Computational Issues in The Planning and Kinematics of Binary Robots". Proceedings of the 2002 IEEE International Conference on Robotics and Automation, Washington D.C. May 2002.
- [7] Lichter, M.D., "Concept Development for Lightweight Binary-Actuated Robotic Devices, with Application to Space Systems" Master's thesis. The Massachusetts Institute of Technology, Cambridge, USA, 2001.
- [8] Hamlin G.J., and Sanderson A.C. "TETROBOT: A Modular Approach to Reconfigurable Parallel Robotics". Kluwer Academic Publishers, 1998.
- [9] Lichter, M.D., Sujan, V.A., and Dubowsky, S. "Experimental Demonstrations for a New Paradigm in Space Robotics". Proceedings of the Seventh International Symposium on Experimental Robotics, ISER '00. Hawaii, pp. 225-234. December 10, 2000.
- [10] Sujan, V.A., Lichter, M.D., and Dubowsky, S. "Lightweight Hyper-redundant Binary Elements for Planetary Exploration Robots". Proc. 2001 IEEE/ASME International Conference on Advanced Intelligent Mechatronics (AIM '01) 811 July 2001, Como, Italy.
- [11] Kumar, P. and Pellegrino, S., "Kinematic Bifurcations in the Simulation of Deployable Structures" IASS-IACM, ISASR, Athens, Greece 2000.
- [12] Madden, J.D., Cush, R.A., Kanigan, T.S., Hunter, I.W. "Fast Contracting Polypyrrole Actuators". Synthetic Metals, Vol. 113 (2000) pp. 185-192.
- [13] Wittrick, W. H., "The Properties of Crossed Flexure Pivots, and the Influence of the Point at Which The Strips Cross". The Aeronautical Quarterly II (4), pp 272-292, 1951.
- [14] Haringx, J. A. "The Cross-Spring Pivot as a Constructional Element", Applied Science Research, pp 313-332, 1949.
- [15] <http://plastics.dupont.com/>
- [16] Hafez, M., Sidler T., Salathe R., Jansen G. and Compter J. "Design, Simulations and Experimental Investigations of a Tip/Tilt Scanner" Mechatronics, 10, 2000 pp. 741-760.
- [17] Hafez, M., "Compact Fast-Steering Tip/Tilt Laser Scanner for High-Power Material Processing Applications" PhD Thesis, The Swiss Federal Institute of Technology, Lausanne, Switzerland, 2000.
- [18] Furlani E. P., "Formula for The Levitation Force Between Magnetic Disks" IEEE Transactions on Magnetics, Vol. 29, No. 6. November 1993.
- [19] Kim K., Levi E., Zabar, Z. and Birenbaum, L., "Restoring Force Between Two Noncoaxial Circular Coils" IEEE Transactions on Magnetics, Vol. 32, No. 2, March 1996.
- [20] Smith S.T., Chetwynd D.G., "An optimized Magnet Coil Force Actuator and its Application to Precision Elastic Mechanisms" Proceedings of the Institution of Mechanical Engineers. Vol. 204, pp.243-253, 1990.
- [21] Compter J. C., "Snelle Aandrijvingen Met Korte Slag – Fast Actuators With Short Strokes" PhD Thesis Technical University of Delft, The Netherlands, 1976.

Computational Issues in the Planning and Kinematics of Binary Robots

Matthew D. Lichter, Vivek A. Sujan, and Steven Dubowsky

{ lichtner | vasujan | dubowsky@mit.edu }

Department of Mechanical Engineering

Massachusetts Institute of Technology

Cambridge, MA 02139 USA

Abstract

To meet the objectives of many future missions, robots will need to be adaptable and reconfigurable. A concept for such a robotic system has been proposed previously based on using a large number of simple binary actuators. Previous researchers have addressed some of the issues brought up by robots with a few binary actuators. This paper examines the computational feasibility of controlling and planning such binary robotic systems with a large number of actuators, including computation of their workspace, forward kinematics, inverse kinematics and trajectory following. Methods are proposed and evaluated by simulation. Detailed error analysis and computational requirements are presented. An example of the planning for a binary walking robot is presented.

1. Introduction

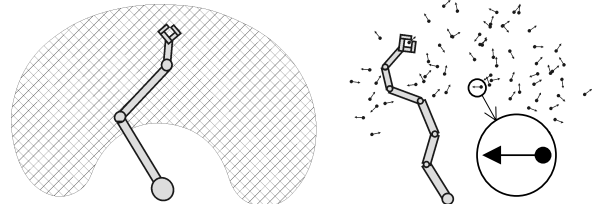
Future robots will be needed to perform complex tasks in difficult environments. For example, missions to Mars will require robots to perform tasks such as scouting, mining, conducting science experiments, and constructing facilities for human explorers and settlers [9]. To accomplish these objectives, robotic systems will need to be lightweight, reliable and robust. Further, the elements of these systems need to be capable of large and fine motion, a large motion workspace, multiple degrees of freedom, and have a small stowed volume. A new design concept has been proposed to meet these challenges [12, 15]. In this concept, robotic systems use tens or hundreds of simple binary actuators embedded in a flexible structures. Each of the binary degrees of freedom contains a bi-stable element so that the actuators simply flip the state of the joint. As the number of binary degrees of freedom in the system increases, the capabilities of the device approach that of a conventional continuous robotic system. This is analogous to the digital computer replacing the analog computer. The control of such devices is rather simple. To achieve a given position a set of joints simply need to be flipped. No feedback is required and theoretically no “servo errors” will exist. Control of such actuators has been classified as sensor-less manipulation [4, 6, 12]. The kinematics and control of such “hyper-redundant” manipulators, both with and without binary actuation have been studied by a number of researchers [1, 3, 7, 8, 12]. However, many of the planning and kinematics issues of binary robots are fundamentally different and more difficult than those of conventional robotics [3, 12, 15]. For example, the inverse kinematics problem for a binary robot involves searching through a discrete set of configurations to find the one that best matches the desired state, rather than solving geometric equations to

determine joint angles or link lengths, as one would do for a continuous systems. Most research has involved binary robotic systems when the number of degrees of freedom is relatively small, in the order of tens of DOF.

This paper describes analysis and simulation studies performed to examine the feasibility of controlling and planning binary-actuated robotic systems in real time when the number of DOF is very large (hundreds or thousands). Such systems are currently under development [16]. The work also suggests planning algorithms that can be used in future systems. The work outlines some of the issues and potential methods for the workspace analysis and optimization, the forward and inverse kinematics, and trajectory planning of binary robotic systems. These methods are then applied to binary systems used for robot locomotion.

2. Workspace Analysis and Optimization

The workspace of a robot generally refers to the locus of all points that a robot’s end-effector can reach [2]. With a continuous system, the workspace is usually a region in continuous space (see Figure 1(a)). Many continuous robots are also able to achieve a continuous range of end-effector orientations for a given point in the workspace. Understanding the size of the workspace as well as the “orientability” of the end-effector within this workspace gives some measure of the ability of the robot to perform diverse manipulation tasks.



(a) continuous robot workspace (b) binary-actuated robot workspace
Figure 1: The distinction between binary and continuous robot workspace

For binary-actuated robots the notion of a workspace takes on some subtle differences [14]. For a binary system, the workspace is not a continuous volume but rather a finite set of points in space (see Figure 1(b)). For each point there is an associated orientation of the end-effector, indicated by the arrows originating from each point in Figure 1(b). In such a workspace one can guarantee the existence of at least one binary configuration of the robot that achieves a minimum error of end-effector position and orientation. Thus for a binary robot, the density of the points within the workspace can be important, since a dense set of points will generally achieve small end-point errors. The density of points increases as the number of actuators in the system

increases. Each additional actuator doubles the number of workspace points.

It is useful to view a discrete workspace cloud from the perspective of a density function map. In designing a binary robot, one might want to optimize its workspace. For example, it may be desirable for repeated pick and place tasks to have a workspace that has a great density of points in the pick and place locations. In other cases, it might be desirable to have a uniform distribution of reachable points over the entire workspace. To deal with such issues the notion of workspace distribution is proposed. For a planar robot, a density map represents the density of points (the z-axis) versus the Cartesian location in space (the x- and y-axes). With a discrete cloud, the density map appears as delta functions at each workspace point, with all other areas of the map having a value of zero density (see Figure 2 (a)). Applying a low-pass filter (such as convolution with a Gaussian function) to the density map, the spikes blend together and provide a continuous approximation of the density of the workspace (see Figure 2(b)).

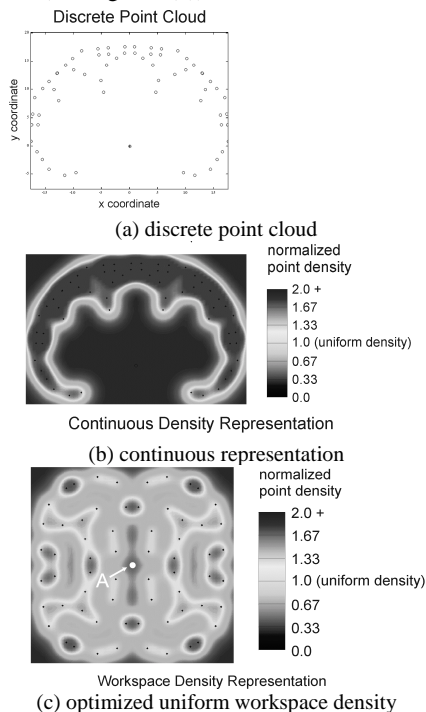


Figure 2: Workspace of a 6 DOF serial binary manipulator with optimization

This continuous approximation can be a metric for the uniformity/distribution of the workspace. Here it is defined based on the standard deviation of the workspace density. A small standard deviation of the workspace density indicates a more uniform distribution. This method for quantifying the distribution of the workspace can be extended to three-dimensional workspaces and include endpoint orientation information.

As an example of optimizing a binary robot design to provide uniform workspace density, consider a serial planar manipulator, having between four and ten binary

actuators. The lengths of each link, l_i , and the angles of deviation of each binary rotary joint, ϕ_i are to be optimized. This robotic design results in a planar workspace composed of 2^N points, where N is the number of binary actuators.

Using an evolutionary algorithm the design variables of this system can be optimized. The algorithm generates a random set of candidate designs and evaluated them based on their uniformity of workspace. The best candidates (those with the most uniform workspace densities) are evolved in the classical manner with mutation. A few hundred generations result in good solutions to the problem. An example of one such optimization (for an un-optimized system shown in figure 2(a)) is shown in Figure 2(c). Note that the density map in this figure is much more uniform than the one shown in Figure 2(b).

3. Kinematics

3.1. Forward Kinematics

For binary robotic systems, it is convenient to formulate the forward kinematics using four-by-four homogeneous transformation matrices [2]. For example, the transformation matrix $A_{0,M}$ describing the position and orientation of the end-effector relative to the base can be viewed as the product of the M intermediate transformations $A_{i-1,i}$ from module to module within the structure:

$$A_{0,M} = A_{0,1} \cdot A_{1,2} \cdot \dots \cdot A_{M-1,M} = \prod_{i=1}^M A_{i-1,i} \quad (1)$$

where M is the number of intermediate modules comprising the binary robotic system [15].

Due to the discrete nature of binary devices, each term of the intermediate transformation $A_{i-1,i}$ can have only a finite number of possible values. If each module has only a few binary degrees of freedom, all the values that the terms of $A_{i-1,i}$ can be easily enumerated. For example, if a module has three binary DOF, then the module has 2^3 or 8 possible values for $A_{i-1,i}$ (notated by $A_{i-1,i}^{(1)}$, $A_{i-1,i}^{(2)}$, ..., $A_{i-1,i}^{(8)}$). The solution of the module kinematics may require trigonometric or more complex mathematics, but these need only be solved once, and possibly offline. This reduces online computational loads.

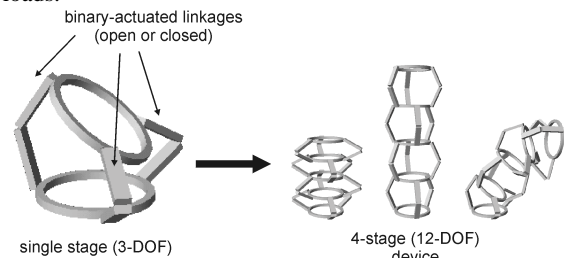
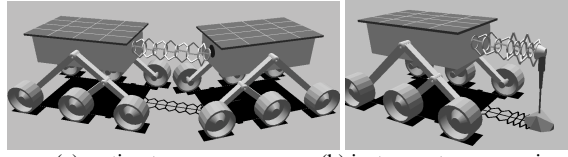


Figure 3: BRAID—a serial chain of binary-actuated parallel stages

An example of such a robot is the Binary Robotic Articulated Intelligent Device (BRAID), developed at the Field and Space Robotics Laboratory, which is a serial stack of identical parallel stages [15] (see Figure 3). Such

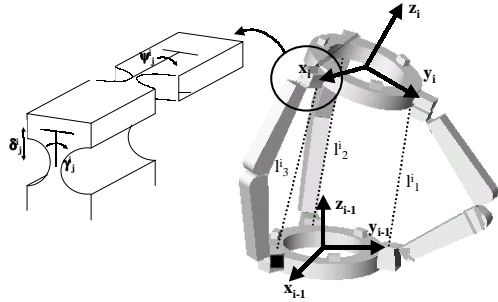
a design could be used for manipulating instruments, collecting soil samples, or mating two cooperating robots, applications that require only moderate precision (see Figure 4).



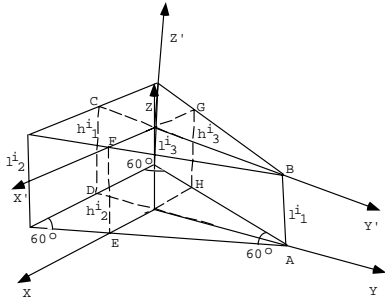
(a) mating two rovers (b) instrument maneuvering
Figure 4: Potential BRAID applications

In a single parallel link stage of the BRAID system, the three legs are positioned about the vertices of two equilateral triangles. Additionally, based on the joint configuration of each leg, the single stage has only three degrees of freedom—pitch (θ_x) and yaw (θ_y) rotations and a vertical (z) translation (coupling effects lead to non-independent motions in the x and y directions as well). The four by four transformation matrix $A_{i-1,i}$, of the i^{th} coordinate frame with respect to the $i-1^{\text{th}}$ coordinate frame is defined based on these five motions. The matrix A_{0M} defines the forward kinematics from base to end-effector of the entire system. In this formulation the leg lengths are the control variables. The relationship between these leg lengths and the pitch, yaw, and translation motions of the i^{th} coordinate frame with respect to the $i-1^{\text{th}}$ coordinate frame is given below. From Figure 5 the deflection parameters (δ^i , γ^i , ψ^i) give us the coupled x^i and y^i translation of the i^{th} stage:

$$x^i = -\delta_1^i \sin(\gamma_1^i) \quad y^i = -\left(\frac{r}{2} - \frac{\delta_3^i \sin \gamma_3^i}{\cos \pi/6} - \frac{r}{2} \cos \theta_x^i \right) \quad (2)$$



(a) Single BRAID module



(b) geometrically equivalent representation

Figure 5: Critical parameter representation of BRAID system

The following relations can be obtained from figure 5:

$$h_1^i \sin \theta_2 - l_1^i \sin \theta_1 = \frac{3}{2} r \sin \theta_x \quad (3)$$

$$h_2^i \sin \alpha_2 - h_3^i \sin \alpha_1 = \frac{2}{\sqrt{3}} r \sin \theta_y \quad (4)$$

where $\theta_1 = \angle DAB$, $\theta_2 = \angle ADC$, $\alpha_1 = \angle EHG$, and $\alpha_2 = \angle FEH$, can be found from the leg lengths l_1^i , l_2^i , and l_3^i . Equations 3 and 4 give two independent equations in two unknowns. However, both are highly non-linear transcendental equations and can only be solved numerically to give the BRAID forward kinematics. A Newton-Raphson algorithm was implemented to solve for the unknowns, θ_x and θ_y . Finally, the vertical translation can be solved using solutions for θ_x , θ_y and equation 5.

$$z^i = h_2^i \sin \alpha_2 - \frac{1}{\sqrt{3}} r \sin \theta_y = h_1^i \sin \theta_2 - \frac{1}{2} r \sin \theta_x \quad (5)$$

3.2. Inverse Kinematics

The planning and execution of practical tasks generally requires the solution to the inverse kinematics problem. The complexity of the trajectory planning and inverse kinematics software of binary devices are more complex than that of continuous systems. The inverse kinematics problem cannot be expressed in a closed form solution. Brute force or exhaustive search methods may prove appealing for systems with few stages (less than 5), but become impractical for larger systems. As the number of degrees of freedom increase, the complexity of the workspace grows exponentially. For example, for every additional stage in the BRAID there is about an order of magnitude increase in the number of states in the workspace. Hence, for large systems more efficient search methods are required to find “optimum” solutions. In this study two search methods for the inverse kinematics problem are studied. The first is a combinatorial search algorithm and the second is a genetic search algorithm. The search metric for both algorithms is to minimize the error between the true end-effector and desired position. Both algorithms are briefly described below.

3.2.1. Search Algorithms

The combinatorial search algorithm was first described in [12]. To avoid exponential growth of the search space as the number of actuators grow, the inverse kinematics are solved by changing the state of only a few actuators at a time. This is perceived as a k -bit change to the given system state, where any system state is defined by an m -bit word (m is the number of binary actuators). At any state all possible changes (of up to k -bits, where $k \leq N$) are evaluated to determine the one that optimizes the search metric (i.e. reduces the error between the end-effector position and the desired position). This optimal change forms the new state of the system and the search procedure repeats until convergence. This reduces the computational complexity from $O(2^N)$ to $O(N^k)$ or from exponential computational time to polynomial computational time [12].

The genetic algorithm used, is a classical one, where each generation consists of N -bit binary words describing

the manipulator state (where m is the number of binary actuators). A full description of genetic algorithms can be found in [5]. Comparing the genetic algorithm to the others discussed, the size of the search space explored by the genetic algorithm is given by:

$$\text{search_space_size} = E \cdot G \cdot P \quad (6)$$

where E is the number of populations separately evolved, G is the number of generations for each population, and P is the number of individuals within the population. In studies done here, E , G , and P were kept constant relative to the number of degrees of freedom, N . For more advanced algorithm development, these values could be made a function of N . Within the algorithm, several computations take place that are linearly proportional to N (such as forward kinematics computations) and therefore computation time of the inverse kinematics using a genetic algorithm grows approximately linearly with the number of DOF of the system.

3.2.2. Algorithm Comparisons

Performance of the two search methods is quantified on a stochastic basis using a Monte Carlo method. One thousand target points with random orientations are selected randomly within the volume of a binary workspace cloud of a multi-staged BRAID system. The targets are chosen from within a spherical region, whose radius is roughly 90% of the radius of the actual point cloud. The inverse kinematics for each target pose is then solved for and the solution times and pose errors are computed and recorded. For comparison, results from exhaustive searching are also presented.

Figure 6 shows the times for solving the inverse kinematics problem for the two algorithms described above. The times were computed from simulations performed on a 600 MHz Pentium III processor. In these studies, the exhaustive search was observed to be the fastest for systems with less than 12 DOF, the combinatorial algorithm was the fastest for systems having between 12 and 40 DOF, and the genetic algorithm was the fastest for larger systems.

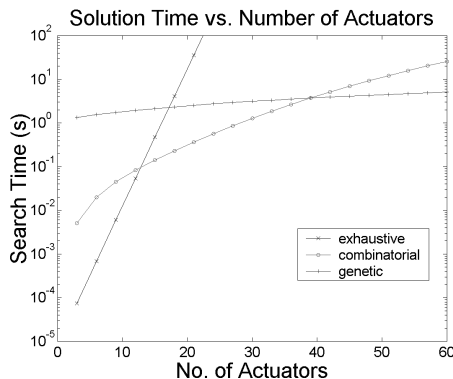


Figure 6: Inverse kinematics algorithms solution times

Errors in position and orientation for the algorithms are also quantified. An example of the distribution of the errors is shown in Figure 7 for the case of a 30 DOF (a 10 stage) BRAID. The shapes of the error distributions for any given BRAID are very similar for each of the

algorithms and most closely resemble a gamma distribution. The outliers are generally near the boundaries of the workspace, and in practice tasks should be planned to avoid these regions.

Figure 8 shows that the median errors drop as a function of the number of DOF for the combinatorial and genetic search algorithms. After about 30 DOF, there are only marginal improvements as the number of DOF increases. For systems with 30 DOF (a ten-stage BRAID), displacement errors are within a few percent of the characteristic manipulator length and angular errors are within fifteen degrees. Such a system is unsuitable for precision work, but may be acceptable for such tasks as camera placement, crude instrument manipulation, and sample collection.

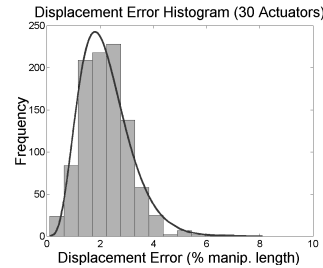


Figure 7: Error distribution for a 30-DOF BRAID: displacement error (1000 samples)

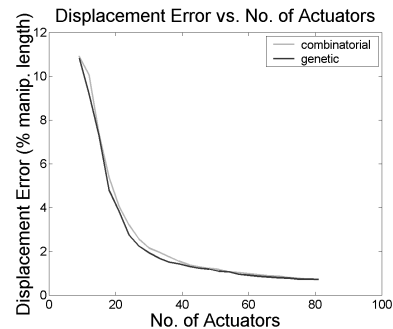


Figure 8: Median errors vs. number of DOF for different algorithms: displacement error (1000 samples per DOF)

4. Trajectory Following

The trajectory following problem is also quite different for a binary device than for continuous ones. Instead of using Jacobian matrices to compute actuator commands [2], the problem is solved by a repeated search through the configuration space to find the configuration whose end-effector most closely matches a moving target [12]. Hence, this problem is very close to the methods described above and can be directly applied. For low-DOF systems, the exhaustive search may prove to be the easiest and most robust method for trajectory following. For systems with higher DOF, genetic algorithms or combinatorial searches would be more effective. However, it was found that the genetic algorithm used is not well suited for trajectory following. A genetic algorithm, given the same target and the same initial conditions, will produce different solutions because of its randomly selected initial population and mutation

component. Since the high DOF system is highly redundant, there can be a large number of configurations that will produce nearly the same end-effector position yet will have greatly different configurations. A relatively smooth path planned in Cartesian space may have an erratic path in configuration space (see Figure 9). For power consumption, reliability, and transient behavior, this is very undesirable.

Hence, the combinatorial search algorithm is found to be the most effective method for trajectory following. This algorithm searches only the subset of neighboring configurations, and generates a path that is relatively smooth in Cartesian and configuration space. Between time steps, only a few (specifically defined) actuators will be actuated at a time. The combinatorial algorithm runs much faster in the trajectory planning problem than for the inverse kinematics problem described in Section 3.2.1, since it only makes one iteration per time step (see Figure 10).

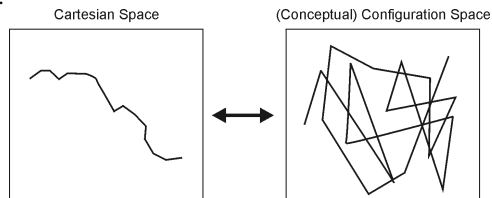


Figure 9: A smooth trajectory in Cartesian space is not necessarily smooth in configuration space

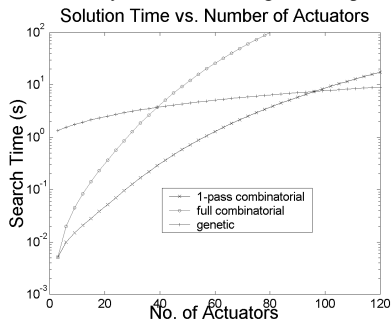


Figure 10: Inverse kinematics solution times for each trajectory following step

Simulations showed that the errors maintained during trajectory following were acceptable for a number of applications such as maneuvering a camera or instrument, or manipulating an object with low precision (see Figure 11). Typical errors during manipulation were found to be of roughly the same size as those discussed in Section 3.2.2.

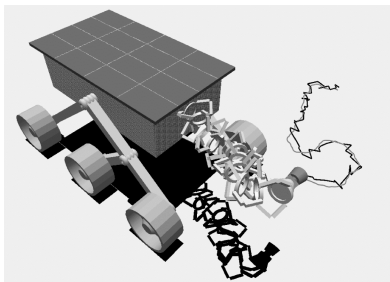


Figure 11: Simulation of a camera maneuvering task—desired trajectory: lighter path; actual trajectory: darker path.

5. Locomotion Planning

The trajectory following problem can be extended to the locomotion planning problem, where binary devices are used as legs. Simulations were done to explore the feasibility of planning actuator sequences in real-time for a robot having six binary-actuated legs walking in rough terrain. Each of the six legs is modeled as a Braid and has 21 binary DOF (see Figure 12), yielding a total of 126 DOF for the system. Desired ground contact points for the legs are chosen and the configurations and actuator sequences are planned to achieve these contact points and body motions.

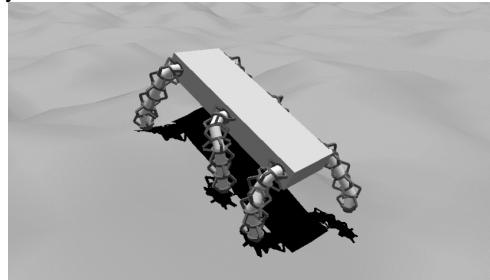


Figure 12: Simulation of a 6x21-DOF walking robot composed of six BRAIDS for legs, walking in rough terrain.

Several issues arise with a binary system for this problem. First, the multiple legs in contact with the ground form a closed kinematic chain that is over-constrained due to the discrete nature of the leg motions. If the ground contact points are rigidly held, it will be impossible for the contacting legs to change configurations due to the incompatibilities between each leg's workspace (see Figure 13(a)). Thus, it is impossible to shift the body while keeping the feet planted, as required for walking. Here a small amount of local compliance in the ground contact is permitted and the limited effects of the incompatibilities between the workspaces of planted legs are ignored (see Figure 13(b)).

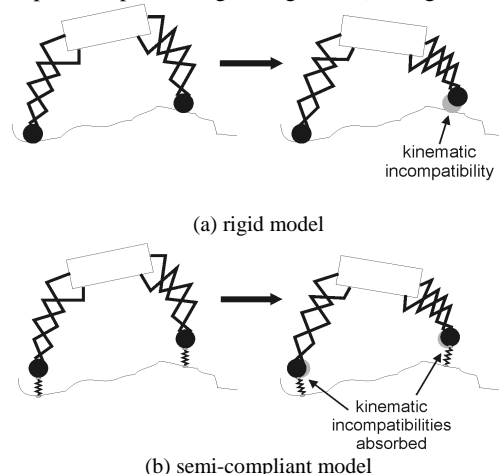


Figure 13: Kinematic models in simulation

A second issue arises in finding the binary configuration of the legs that allows the body to move in a prescribed manner. The system can be considered as a single parallel 126 DOF system with ground contact points modeled as continuous revolute joints with

displacement compliance. With the requirement that trajectories are smooth in both Cartesian and configuration space, this system becomes computationally difficult to solve quickly. To simplify this locomotion-planning problem, each leg was viewed as an independent trajectory planning problem. First, the desired position of the body for the next small time step is selected. Then, the inverse kinematics for each leg is solved using the one-pass combinatorial algorithm to make the leg move to the desired ground contact point.

With the configuration of each leg being solved independently, the actual body position does not coincide exactly with the desired body position. The actual body position is obtained from the equilibrium condition of the compliant contact elements on the fixed configuration robot. This problem is solved by minimizing the potential energy stored in the compliant elements as a function of final body position. The error requiring adjustments is small, roughly the size of the errors in the legs themselves, generally a few percent of the characteristic size (see Section 3.2.2). For most applications, these errors would be acceptable.

This planning method is found to be effective and fast. Using a Pentium III 933 MHz processor, the simulated robot plans and executes a stride at a rate of once per second. The robot is able to execute side-stepping and turning motions in rough terrain. It maintains static stability while walking on slopes up to 20 degrees. Static stability is only lost occasionally ascending, descending, and traversing very steep slopes of around 45. This loss of stability would need to be addressed by the high-level planner of the robot [11]. This requirement would be the same for robots with continuous degrees of freedom.

6. Conclusions

This paper considers some of the computational challenges for the planning of binary robotic systems. The notion of a binary workspace optimization was described. The forward kinematics of binary systems was discussed, and the computational simplicity of this operation relative to continuous systems was shown. The methods to solve the inverse kinematics and trajectory planning were addressed and compared to those of continuous systems. The positioning errors of binary systems were also quantified in a probabilistic manner. The methods were applied to a walking system that might be used for future space exploration.

Acknowledgements

The authors would like to acknowledge the NASA Institute of Advance Concepts (NIAC) for their support in this work.

References

[1] Chirikjian, G.S.; Burdick, J.W. *The kinematics of hyper-redundant robot locomotion*. IEEE Transactions on Robotics and Automation. Volume: 11 Issue: 6, Dec. 1995 Page(s): 781 –793

[2] Craig J.J. *Introduction to Robotics: Mechanics and Control*. Second ed, Addison-Wesley, Reading, MA, 1989.

[3] Ebert-Uphoff, I.; Chirikjian, G.S. *Inverse kinematics of discretely actuated hyper-redundant manipulators using workspace densities*. Proceedings of the IEEE International Conference on Robotics and Automation, 1996, Volume: 1, Page(s): 139 -145 vol.1.

[4] Erdmann, M.A. and Mason, M.T. *Exploration of sensor-less manipulation*. IEEE Journal of Robotics and Automation, Vol. 4, pp 369-379, August 1988.

[5] Goldberg, D. *Genetic Algorithms in Search, Optimization, and Machine Learning*. Addison-Wesley, Reading, MA 1989.

[6] Goldberg, K. *Orienting polygonal parts without sensors*. Algorithmica, 1992, Special Robotics Issue.

[7] Huang, M.Z., Shou-Hung Ling. *Kinematics of a class of hybrid robotic mechanisms with parallel and series modules*. Proceedings of the 1994 IEEE International Conference on Robotics and Automation, Page(s): 2180 -2185 vol.3.

[8] Hughes, P.C. *Trussarm – a variable geometry truss manipulator*. Journal of intelligent materials, systems and structures, vol. 2, pp. 148-160, April 1991.

[9] Huntsberger, T.L., G. Rodriguez, and P. S. Schenker. *Robotics: challenges for robotic and human Mars exploration*. Proceedings of ROBOTICS2000, Albuquerque, NM, Mar 2000.

[10] Kwon, S., Youm, Y. *General algorithm for automatic generation of the workspace for n-link redundant manipulators*. Proceedings of the International Conference Advanced Robotics, 1991. 'Robots in Unstructured Environments', Page(s): 1722 -1725 vol.2.

[11] Latombe J. *Robot Motion Planning*. Kluwer Academic Publishers, Boston, MA 1991.

[12] Lees, D.S. and Chirikjian, G.S. *A combinatorial approach to trajectory planning for binary manipulators*. Proceedings of the IEEE International Conference on Robotics and Automation, Minneapolis, Minnesota, April 1996.

[13] Lichter, M.D., Sujan, V.A., Dubowsky, S. *Experimental Demonstrations of a New Design Paradigm in Space Robotics*. Proceedings of the Seventh International Symposium on Experimental Robotics, ISER 00. Dec 10-13, 2000, Honolulu, Hawaii.

[14] Sen D, Mruthyunjaya T S. *A Discrete State Perspective of Manipulator Workspaces*. Mech. Mach. Theory, Vol. 29, No.4, 591-605, 1994.

[15] Sujan, V.A., Lichter, M.D., and Dubowsky, S. *Lightweight Hyper-redundant Binary Elements for Planetary Exploration Robots*. Proceedings of the 2001 IEEE/ASME International Conference on Advanced Intelligent Mechatronics (AIM '01). 8–11 July 2001, Como, Italy.

[16] Hafez, M., Lichter, M.D., and Dubowsky, S. *Optimized Binary Modular Reconfigurable Robotic Devices*. Proceedings of the 2002 IEEE International Conference on Robotics and Automation. Washington, D.C., May 11-15, 2002.

Experimental Demonstrations of a New Design Paradigm in Space Robotics

Matthew D. Lichter, Vivek A. Sujan, and Steven Dubowsky
Department of Mechanical Engineering
Massachusetts Institute of Technology
Cambridge, MA 02139 USA
{lichter | vasujan | dubowsky} @mit.edu

Abstract: This paper presents a study to experimentally evaluate a new design paradigm for robotic components, with emphasis on space robotics applications. In this design paradigm, robotic components are made from embedded binary actuators and compliant mechanisms in order to reduce weight and complexity. This paper presents a series of five experiments that demonstrate the concept. These studies include a reconfigurable rocker suspension for rocker-bogie rovers, a sample acquisition gripper, a pantograph mechanism for robotic legs, an articulated binary limb, and a hyper-degree-of-freedom mechanism building block.

1. Introduction

Future missions to planets such as Mars will require explorer/worker robots to perform tasks of increased complexity such as exploring, mining, conducting science experiments, constructing facilities, and preparing for human explorers. To meet the objectives of missions in the year 2010 to 2040 timeframe, planetary robots will need to work faster, travel larger distances, and perform highly complex tasks with a high degree of autonomy [1]. They will also need to cooperate in teams and reconfigure themselves to meet their mission objectives. Current electromechanical technologies of motors, optical encoders, gears, bearings, etc. will not be lightweight and robust enough for these robots.

In this research, a new class of building blocks for planetary robots is being studied. These devices, called Articulated Binary Elements (ABEs), consist of compliant mechanisms with large numbers of embedded actuators and sensors. Figure 1 shows two concepts of the ABE elements. These actuators would be binary (on/off) in nature and could be made from conducting polymer, electrostrictive polymer artificial muscle, shape memory alloy, etc. [2,3]. By using hundreds or thousands of very simple but reliable actuators, one can approximate a continuous robotic system in dexterity and utility. This is analogous to the leap from analog to digital computing. The advantage of binary actuation is the fact that systems can be controlled in the absence of feedback sensing and using only very simple digital electronics, due the robust nature of a two-state actuator. In this work, the feasibility of the ABE concept for planetary robots is being studied analytically and experimentally.

This paper presents an overview of a series of five experimental developments performed to establish credibility and feasibility of the concepts of embedded binary

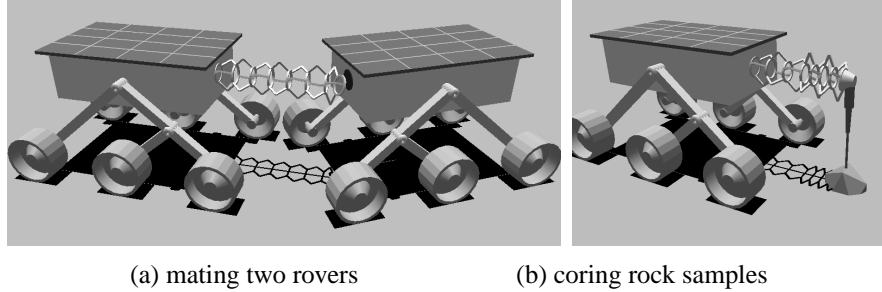


Figure 1. Two ABE robotic potential applications.

actuation and elastic robotic elements. They are a reconfigurable rocker suspension for rocker-bogie rovers, a science sample gripper, a pantograph mechanism for a robot leg, an articulated binary limb, and a hyper-degree-of-freedom mechanism building block. Each of these case studies suggests that light weight and simple robotic elements can be constructed with this design paradigm. The work also highlights several limitations that will need to be overcome for the concept to reach its full potential.

2. Background and Literature

The concept of binary robotics is not altogether new. In the 1960's and 70's sporadic work was done in areas of binary actuation and sensorless robotics [4,5]. Deeper study of this area did not occur until recently [6-10], when computation power made the analysis, control, and planning for binary robots feasible.

Solving the forward and inverse kinematics, in order to follow trajectories for a binary robot, is a very different problem than that for a continuous robot. Because the actuators can achieve only finite displacements, a binary robot can reach only finite locations and orientations in space. The workspace of a binary robot is thus a point cloud and the inverse kinematics problem becomes simply a search through this cloud. However, for large numbers of actuators this search space explodes rapidly (the number of search points is 2^N , where N is the number of actuators). Methods for solving these computational challenges have been developed [8-10]. The most common methods reduce the search space through a combinatorial approach or use stochastic searches such as genetic algorithms.

Some experimental work has been done on binary redundant manipulators [8]. An example is a variable-geometry truss (VGT) manipulator that was constructed using pneumatic actuators which were overpowered and held at their stops. These studies showed the fundamental ability of binary robots to perform some tasks. Such devices constructed using conventional components cannot demonstrate the full advantages of binary robotic devices, such as achieving large redundancy with simple implementation. To date, little work has been done to experimentally demonstrate simple, lightweight, robust binary designs that are able to perform effectively.

The focus of this work is to study the issues within the context of the application of binary elements in space robots. Binary-actuated elements have great appeal for this area because they can be designed at a fraction of the weight, complexity, and volume of conventional continuously-actuated elements (i.e. motors, hydraulics,

etc.) [2,3]. Incorporating the concept of compliant mechanisms enables further design simplifications through the use of elastic flexures in place of mechanical hinges, bearings, and lubrication. The results of this paper suggest that given the development of high-performance smart materials and artificial muscle technology, a whole new realm of robotics design will emerge.

3. Technology Demonstrations

3.1. Approach

The goal of this research is to investigate and demonstrate the concept and technologies of achieving high degree of freedom binary systems with physically simple and robust implementations. In this concept the actuators are assumed to be polymer-based materials. These materials include conducting polymers [2] and electrostrictive polymers [3]. However, while these materials are anticipated to meet the needs of the concept in the future, they have not yet reached a sufficient state of development to perform practical experimental demonstrations in devices today. For example, conducting polymers require immersion in an ion solution and provide only small displacements. So for this research shape memory alloys (SMAs) were chosen as surrogate actuator material.

In all the devices studied, the challenge was to amplify the very small displacements provided by the muscle-type actuators. The ABE systems described in this paper run the range from one-DOF devices to many-DOF systems which use embedded actuators and continuously compliant structures.

3.2. Case Studies

3.2.1. Reconfigurable Rocker Suspension

When traversing slopes, a rover can greatly increase its tip over stability by changing the spread angle of its rockers θ (see Figure 2) [11]. To examine the concept of achieving this with binary actuation, an SMA-actuated rocker was designed and developed (see Figure 3) [12]. The working prototype has demonstrated the feasibility and simplicity of such a design. While this first experiment uses conventional bearings and structural materials, it shows that binary muscle-type actuation in its simplest form can be effective.

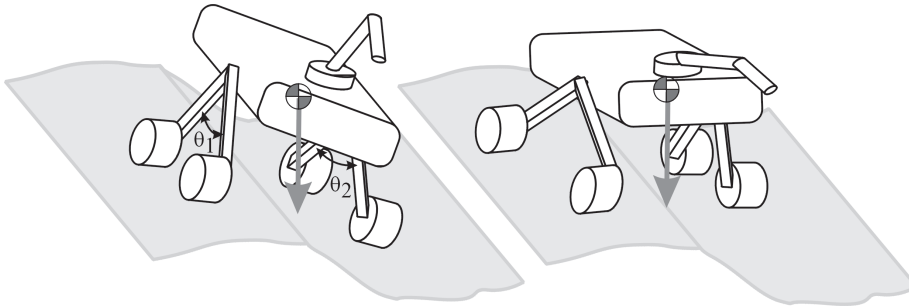


Figure 2. Rover increases tip over stability by reconfiguring its rocker angles θ_1 , θ_2 .

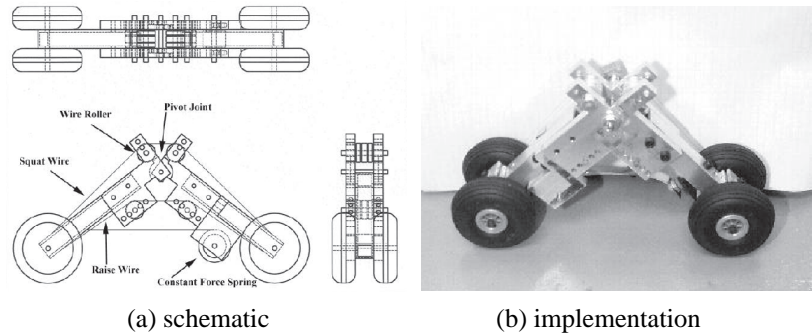


Figure 3. Reconfigurable rocker.

The working prototype has the performance capabilities required for a real rover design. The rocker angle has approximately a 60 degree range of motion (expanding the rocker angle from 90 degrees to about 150 degrees). This results in a change in height of the pivot point of 2.75 cm. The lightweight SMAs allow the rocker to lift a 10 kg payload, half the weight of the rover it was designed for. Actuation takes 0.5 seconds and consumes less than 1.9 W peak. PID control of the SMAs was also studied to examine continuous (non-binary) operation, with good results.

3.2.2. Binary Gripper

In this second device the conventional bearings were replaced by elastic flexure hinges. A one degree-of-freedom binary gripper was designed to show the light weight, simplicity, and utility of the design concept [12]. This gripper could be used for rock sample collection on a space explorer. The gripper has been used for this purpose on a laboratory rover test bed [13].

When the single SMA wire is actuated, the fingers of the gripper close around the object to be grasped (see Figure 4). The key of the gripper design was to amplify the small (5%) deformations of the SMA actuator to be large enough to grasp rock

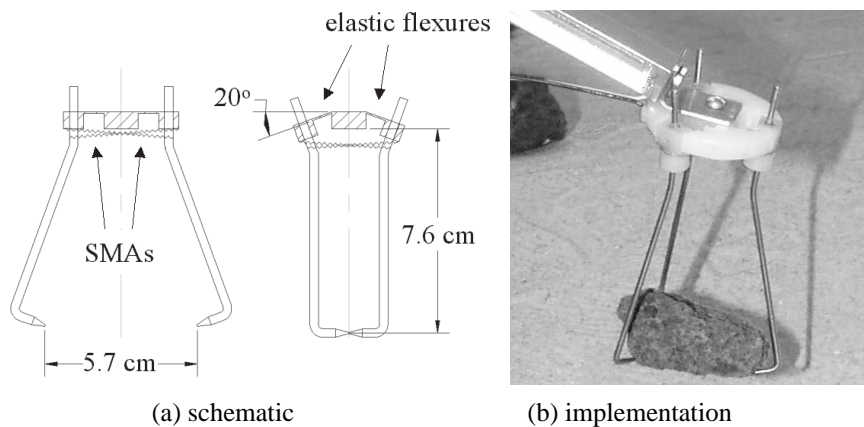


Figure 4. Binary gripper.

samples, while keeping forces at a usable level. Elastic flexures are incorporated at all three finger pivots. The compliance of these flexures acts as a return spring to open the fingers upon release of the object. This device uses no sensors, bearings, or gears.

The gripper with its needle-like fingers and simple binary action is able to reliably grasp rocks of varying size. The mounting base dimension is 2.5 cm in diameter. Each finger is 7.6 cm long, with a motion range of 20 degrees, and can pick up objects up to 5.7 cm in diameter. It can provide a normal force of up to 0.110 N and 0.0422 N at each finger tip, with a 250 micron and 150 micron SMA wire respectively. The expected normal force is 0.149 N and 0.0536 N for the 250 micron and 150 micron wires respectively. The difference in observed versus expected forces can be attributed to wire slip at mounting points, slop in the wire, etc. These observed forces result in reliably lifting objects weighing up to 330 g, six times its own weight of 55 g.

3.2.3. Pantograph Mechanism

A single DOF 4-bar pantograph mechanism was designed to demonstrate large amplification of binary muscle actuator motion (see Figure 5). This amplification is required by some ABE applications, such as legged walking machines.

The pantograph mechanism exemplifies some of the advantages of using compliant members and is an advance over the previous devices considered. The mechanism is simple, since the flexures and bars can be molded or cut from a single piece of material. In this case, a laser cutter was used to cut the part from sheet plastic (PETG — polyethylene terephthalate, glycol modified), although other methods could have been used. Like the previous two studies, this mechanism demonstrates how very small actuator motions can be amplified to usable scales in designs. Although SMA actuator technology can achieve usable elongations of only a few percent, this design can amplify this displacement by a factor of 8 in theory. In the working prototype, the endpoint deflected 29 mm given an actuator contraction of only about 4.5 mm, yielding an amplification of 6.5. The difference between theory and implementation is due mostly to un-modeled compliance in the bars and in irregularities in the SMA actuators.

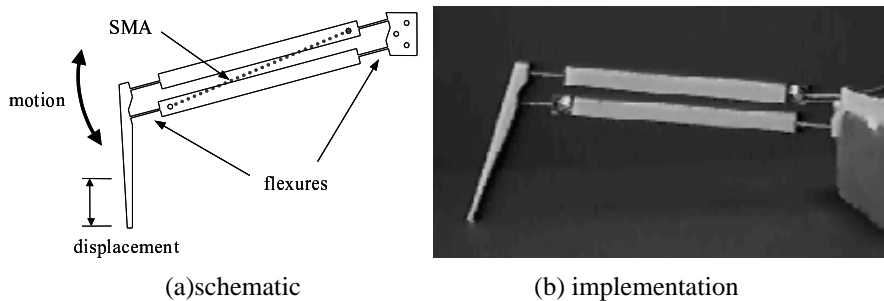


Figure 5. Binary pantograph mechanism.

3.2.4. Articulated Binary Limb (ABL)

A more general Articulated Binary Limb (ABL) was designed to study some of the issues involved with multi-DOF robotic systems [14]. The ABL could be used in a wide variety of space robotic applications, as a dexterous manipulator, as a cam-

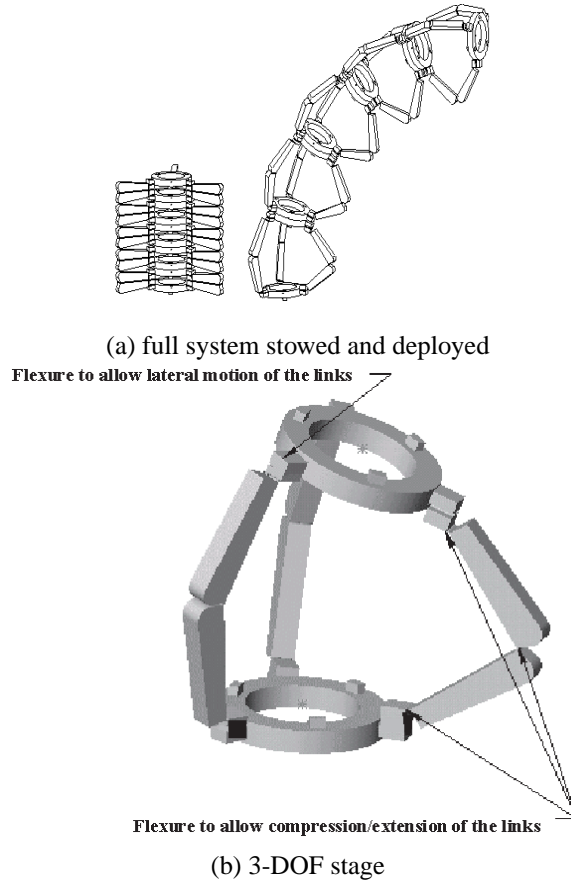
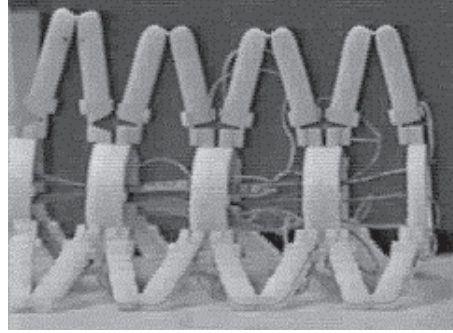


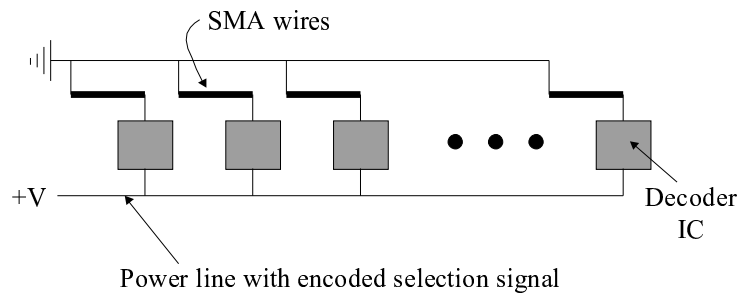
Figure 6. Articulated Binary Limb (ABL).

era or instrument mount, as an articulated connection between cooperating robotic explorer/workers, etc. (see Figure 1). This device is comprised of a serial chain of parallel stages (see Figure 6). In the experimental implementation, each 3-DOF stage is composed of three 1-DOF links, each with a shape memory alloy (SMA) actuator. The links are fabricated from polyethylene using high precision water jet cutting. The link shape provides for an elastic hinge at the end of each element. The actuation scheme allows for only binary operation of each link. The experimental structure built consists of five parallel stages, yielding 15 binary degrees of freedom. The ABL is thus able to achieve $2^{15} = 32,768$ discrete configurations. With this many configurations, the device can approximate a continuous system in dexterity and utility. By its polymer construction and binary actuation the design is very lightweight and simple.

In order to actuate and control such a system, based on the desired kinematics, power must be applied to each actuator by a central controller. The large number of actuators can rapidly make the physical realization of such a system difficult, if each actuator requires an individual set of power supply lines from the central controller



(a) implementation



(b) power bus architecture

Figure 7. Articulated Binary Limb implementation and control.

(see Figure 7a). This multitude of wires adds unacceptable weight and complexity. In this study, a more effective control architecture has been designed (see Figure 7b). A common power line and ground runs between all of the actuators. The power signal is encoded with a high-frequency component that instructs which actuators to turn on or off. Each actuator has a small decoder chip that can be triggered into either binary state by the carrier signal piggybacked on the power line. The carrier signal is a sequence of pulses that identifies a unique address in the form of a binary word. Once triggered, the decoder chip stays latched to that state until triggered otherwise. This power bus architecture reduces the wiring of the entire system to only two wires (power and ground) and can easily be implemented in the form of conducting paint/tape (on the non-conducting polyethylene substrate) to minimize the structural disturbance forces due to wiring.

A key element of the ABE concept is the bi-stable structure. The devices above do not have true bi-stable character in that they depend on actuator forces to hold them in position. To keep a binary actuator in a fixed state often requires power. In order to eliminate this need for continuous power supply and save energy, bi-stable or locking mechanisms can be employed in binary mechanisms to lock the mechanism into each state. In this study methods for bi-stability have been developed. One of the more successful designs is shown below (see Figure 8). This design is comprised of bi-stable mechanisms sandwiched by flexure beams. The bi-stable mechanisms use

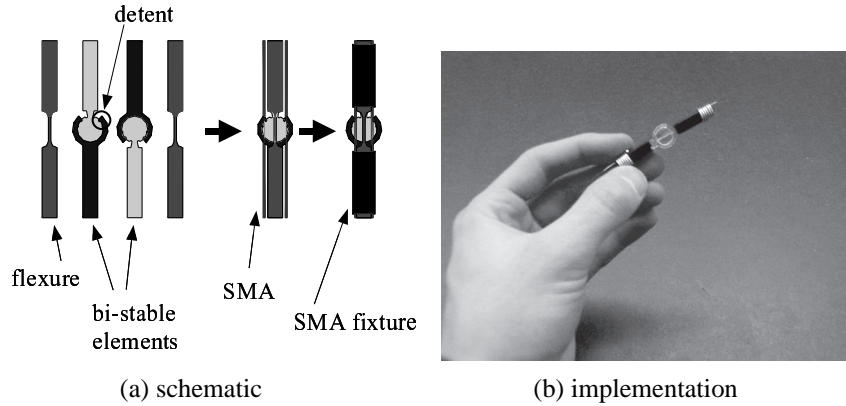


Figure 8. Bi-stable mechanism.

detents to passively lock the joint into discrete states, while the flexures add out-of-plane rigidity. The actuators can be mounted to the sides of a joint like this, similar to the musculature of a human elbow or knee. Fabrication of these bi-stable elements into the hinges of the ABL (shown in Figure 6) is currently under development.

3.2.5. Hyper-DOF Mechanisms

In the progress of developing the ABE concept, continuously compliant structures with embedded actuators are being studied with the aim of understanding a basic building block for more complex designs [15]. Embedding a large number of actuators into a continuously compliant structure can achieve unique motion amplifications and shape deformations (see Figure 9). A mechanism with a cellular structure of hundreds of small deformable cells may provide high performance and large ranges of motion.

Structural finite element analyses have been done of various shapes for individual structures, such as beam elements with voided interior volumes, diamond shaped elements, dog legged elements, elbow elements, and hexagonal elements (see Figure 10). This analysis shows the strong relationship between the structure shape and deformation of the elements.

The manufacture of these elastic elements with embedded actuation is not trivial. In our studies, compliant structures have been cast using different elastomeric materials (see Figure 11). Future work will consider such methods as stereolithography or selective laser sintering as possible alternative fabrication methods.

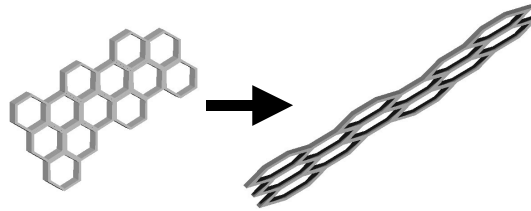


Figure 9. Hyper-DOF network of cells achieving large displacements.

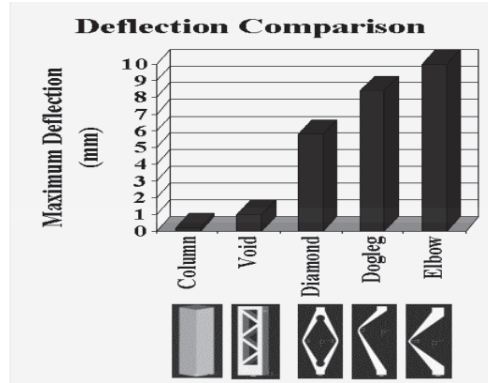


Figure 10. Expected results for various structures.

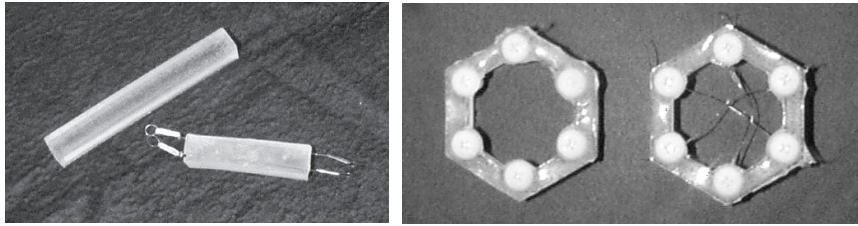


Figure 11. Hyper-DOF systems: flexible structures with embedded SMAs.

4. Summary

This paper presents an experimental study of a new paradigm for the design and fabrication of robotic components, with attention to potential space robotics applications. These robotic components would use embedded binary actuators and elastic members with bi-stable elements. These components have the potential to be implemented with a fraction of the weight, volume, cost, and complexity of conventional systems composed of motors, bearings, geartrains, and encoders. The results of this study suggest that these devices would be effective for robotic systems that are capable of accomplishing space missions of substantial complexity, with flexibility and robustness. The concept is currently limited by polymer actuator development, where present technologies possess practical limitations such as high power requirements, low displacements, or the need for immersion in solutions.

Acknowledgements

The authors would like to acknowledge the NASA Institute for Advanced Concepts (NIAC) for supporting this research. Also the important contributions of Kate Andrews, Robert Burn, and Guillermo Oropeza (students at MIT) and Sharon Lin (research engineer) are acknowledged.

References

- [1] Weisbin C, Rodriguez G, Schenker P, et al 1999 Autonomous Rover Technology for Mars Sample Return. *International Symposium on Artificial Intelligence, Robotics and Automation in Space (i-SAIRAS'99)*, 1-10
- [2] Madden J D, Cush R A, Kanigan T S, et al 2000 Fast-contracting Polypyrrole Actuators. *Synthetic Metals*, 113: 185-193
- [3] Pelrine R, Kornbluh R, Pei Q, et al 2000 High-speed Electrically Actuated Elastomers with Over 100% Strain. *Science*, Vol. 287, No. 5454, 836-839
- [4] Anderson V C, Horn R C 1967 Tensor Arm Manipulator Design. *ASME paper*, 67-DE-57
- [5] Roth B, Rastegar J, Scheinman V 1973 On the Design of Computer Controlled Manipulators. *First CISM-IFTMM Symposium on Theory and Practice of Robots and Manipulators*, 93-113
- [6] Goldberg K 1992 Orienting Polygonal Parts Without Sensors. *Algorithmica*, special robotics issue
- [7] Canny J, Goldberg K 1993 A RISC Paradigm for Industrial Robotics. *Tech. Rep. ESCR 93-4/RAMP 93-2*, Engineering Systems Research Center, University of California at Berkeley
- [8] Chirikjian G S 1994 A Binary Paradigm for Robotic Manipulators. *Proc. IEEE International Conf. on Robotics and Automation*, 3063-3069
- [9] Ebert-Uphoff I, Chirikjian G S 1996 Inverse Kinematics of Discretely Actuated Hyper-Redundant Manipulators Using Workspace Densities. *Proc. IEEE International Conf. on Robotics and Automation*, 139-145
- [10] Lees D S, Chirikjian G S 1996 A Combinatorial Approach to Trajectory Planning for Binary Manipulators. *Proc. IEEE International Conf. on Robotics and Automation*, 2749-2754
- [11] Iagnemma K, Rzepniewski A, Dubowsky S, et al 2000 Mobile Robot Kinematic Reconfigurability for Rough-Terrain. *Proceedings of the SPIE Symposium on Sensor Fusion and Decentralized Control in Robotic Systems III*
- [12] Burn R D 1998 Design of a Laboratory Test Bed for Planetary Rover Systems. Master Thesis, Department of Mechanical Engineering, MIT
- [13] Iagnemma K, Burn R, Wilhelm E, et al 1999 Experimental Validation of Physics-Based Planning and Control Algorithms for Planetary Robotic Rovers. *Proceedings of the Sixth International Symposium on Experimental Robotics, ISER '99*
- [14] Oropeza G 1999 The Design of Lightweight Deployable Structures for Space Applications. Bachelor Thesis, Department of Mechanical Engineering, MIT
- [15] Andrews E K 2000 Elastic Elements with Embedded Actuation and Sensing for Use in Self-Transforming Robotic Planetary Explorers. Master Thesis, Department of Mechanical Engineering, MIT.

Visually Built Task Models for Robot Teams in Unstructured Environments

Vivek A. Sujan and Steven Dubowsky
(vasujan[dubowsky@mit.edu])
Department of Mechanical Engineering
Massachusetts Institute of Technology
Cambridge, MA 02139

Abstract

In field environments it is not usually possible to provide robotic systems with valid geometric models of the task and environment. The robot or robot teams will need to create these models by performing appropriate sensor actions. Here, an algorithm based on iterative sensor planning and sensor redundancy is proposed to enable them to efficiently build 3D models of the environment and task. The method assumes stationary robotic vehicles with cameras carried by articulated mounts. The algorithm uses the measured scene information to find new camera mount poses based on information content. Issues addressed include model-based multiple sensor data fusion, and uncertainty and vehicle suspension motion compensation. Simulations show the effectiveness of this algorithm.

1. Introduction

An important goal of robotics research is to develop mobile robot teams that can work cooperatively in unstructured field environments, such as shown conceptually in Figure 1 [2, 7]. Potential tasks include explosive ordnance removal, de-mining and hazardous waste handling, exploration/development of space, environment restoration, and construction [2, 7, 15].

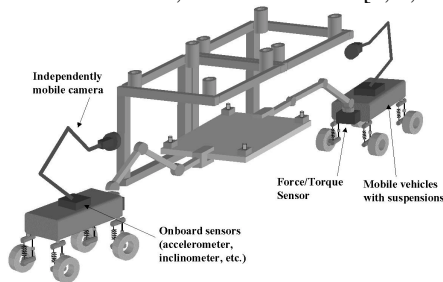


Figure 1: Representative physical system

The control of such systems typically requires models of the environment and task. In unstructured field environments it is often not possible to have such a-priori models. In such cases, the robot needs to construct these from sensory information. A number of problems can make this non-trivial. These include the uncertainty of the task in the environment, location and orientation uncertainty in the individual robots, and occlusions (due to obstacles, work piece, other robots). If the systems are equipped with cameras mounted on articulated mounts, intelligent planning of the camera motion can alleviate problems of the occlusions, providing an accurate geometrical model of the task and environment. If the system consists of more than one robot, planning the behavior of these multi-information sharing systems can further improve the system performance.

Previous work in planning of visual sensing strategies can be divided into two areas [12, 18]. One of these is concerned with sensor positioning—placing a sensor so that it can best observe some feature and selecting a sensing operation which will prove the most useful in object identification and localization. Researchers have limited their work to model-based approaches, requiring previously known environments [4, 6, 9]. Target motions (if any) are assumed to be known. Brute force search methods divide the entire view volume into grids, octrees, constraint sets, and search algorithms for optimum sensor location, are applied [5, 6, 12]. Additionally, they require a-priori knowledge of object/target models [18]. Such methods can be effective but are computationally expensive and not practical for many real field environments, where occlusions and measurement uncertainties are present.

The other direction of research in planning of sensors is sensor data fusion—combining complementary data from either different sensors or different sensor poses to get an improved net measurement [17, 18]. The main advantages of multi-sensor fusion are the exploitation of data redundancy and complementary information. Common methods for sensor data fusion are primarily heuristic (Fuzzy logic) or statistical in nature (Kalman and Bayesian filters) [3, 12, 14].

For environment and target model building both areas play key roles. However, little work has been done in effectively combining the capabilities of sensor placement planning and sensory fusion, to develop a sensing strategy for model building to be used by robots and robot teams in unstructured environments. Some studies have considered cooperative robot mapping of the environment [8, 13, 19]. Novel methods of establishing/identifying landmarks and dealing with cyclic environments have been introduced for indoor environments [8, 19]. In some cases, observing robot team members as references to develop accurate maps is required [13]. Mapping has been done in sequential brute force fashion [13, 19]. Researchers have addressed the concept of map building using a single mobile vision system [1, 4, 10]. Often, sensor models and data uncertainty are not fully considered [1, 10, 11] or exploration schemes are not developed [3, 14]. Structured environment and partial knowledge assumptions are also made [4, 14].

This paper proposes an environment and task model building algorithm, to overcome the uncertainties in robot and camera location and orientation, for robot teams cooperatively working in an unstructured field environment. It is assumed that dimensional geometric information is relevant and required for robots to perform their operations, such as the construction of field

facilities. It is also assumed that the system consists of two (or more) mobile robots working in an unknown environment (such as constructing a planetary structure—see Figure 2). There are no physical interactions between the robots. The vehicles and target are static. Each has a 3D vision system mounted on an articulated arm. Sensing and sensor placement is limited, resulting in occlusions and uncertainties. Again, the objective is to efficiently build a geometrically consistent dimensional model of the environment and target, available to all robots, to allow for tasks to be performed. This involves locating the robots and mapping a region around a target with respect to some target fixed reference frame. The key idea is that the algorithm builds an environment and task model by fusing the data available from each individual robot, providing both improved accuracy as well as knowledge of regions not visible by all robots. Using this algorithm, the individual robots can also be positioned “optimally” with respect to the target [20]. However, this is beyond the scope of this paper.

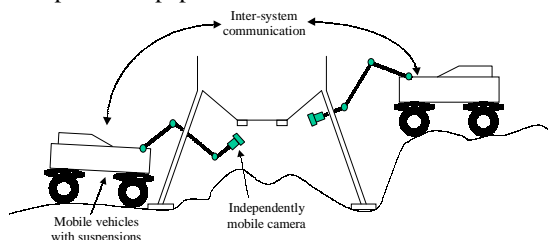


Figure 2: Cooperative mapping by robots

2. Algorithm description

2.1. Overview

The first step in cooperative model building is to visually construct a model of the local environment, including the locations of the task elements and the robots themselves. We assume that only the geometry of the task elements (such as the parts of a solar panel that needs to be assembled [7]) is well known. Obstacles and robot positions are not known.

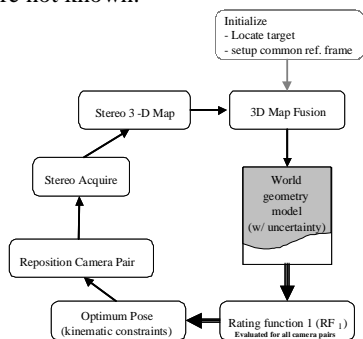


Figure 3: Outline of model building and placement algorithm

Figure 3 outlines the map building algorithm. The algorithm consists of two major parts. In the first part, the articulated cameras cooperatively scan the region around a target generating a 3D geometric model, so that the robots can locate themselves and the obstacles in the target reference frame. The second stage consists of using this model to find an optimum pose for the multiple camera systems to view the target(s). The 3D map is modeled as a probabilistic discretized occupancy grid.

Every voxel in the map has a value for probability-of-occupancy that ranges from 0 (empty) to 1 (occupied). A value of 0.5 indicates maximum uncertainty in occupancy of the voxel. The process is initialized by visually finding the target and robots in a common reference frame. This is done by “looking around” and matching the known target element geometric model with visual data. Next, a new camera pose is found for each of the cameras by defining and evaluating a rating function (RF) over the known environment map subject to kinematic constraints of the sensor placement mechanisms for the individual robots. Then, the cameras move to their new poses and acquire 3D data. Based on the camera mount kinematics, the motions of the cameras are known. Note, it is assumed that the vehicles don’t move, as large camera motions would be difficult to measure. Small motions of the robot base (due to suspension compliance) and errors in camera mounts lead to additional uncertainties. These are accounted for by measuring common features during the camera motion (section 2.5). Finally, the new data and its associated uncertainty are fused with the current environment map resulting in an updated probabilistic environment map.

2.2. Algorithm initialization

As described above, a common target is to be located to establish a common inertial reference frame between the robots and the environment. Searching for the target by moving the robot cameras can be done in many ways (depending on the target properties), such as exhaustive raster scanning, random walking, tracking “space filling curves”, and model-based image understanding methods [12, 18]. In this study, camera positioning for target searching is done in the same way as camera positioning for environment model building (described in sections 2.4).

2.3. Data modeling and fusion

At any time, the cameras on each mobile robot can only observe a small part of their environment. However, measurements obtained from multiple viewpoints can provide reduced uncertainty, improved accuracy, and increased tolerance in estimating the location of the observed object [17]. To fuse multiple range measurements of a feature by sensors, a statistical model of sensor uncertainty is employed (see Figure 4). Current and previous range sensor measurements and their uncertainty models can be integrated to give an updated probabilistic geometric model of the environment.

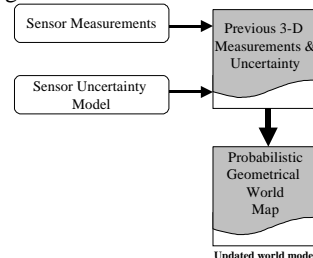


Figure 4: 3-D range measurement fusion with sensor uncertainty

A single range observation of a point (\bar{x}) is modeled as a 3-D Gaussian probability distribution centered at \bar{x} , based on two important observations. First, the use of the

mean and covariance of a probability distribution function is a reasonable form to model sensor data and is a second order linear approximation [17]. This linear approximation corresponds to the use of a Gaussian (having all higher moments of zero). Second, based on the central limit theorem, the sum of a number of independent variables has a Gaussian distribution regardless of their individual distributions.

The standard deviations along the three axes of the distribution correspond to estimates of the uncertainty in the range observation along these axes. These standard deviations are a function of intrinsic sensor parameters (such as camera lens shape accuracy) as well as extrinsic sensor parameters (such as the distance to the observed point or feature). This model can be theoretically approximated as [20]:

$$\sigma_{x,y,z} = f(\text{extrinsic parameters, intrinsic parameters}) \quad (1)$$

$$\approx S \cdot T_{x,y,z} \cdot d^n$$

where S is an intrinsic parameter uncertainty constant, $T_{x,y,z}$ is an extrinsic parameter uncertainty constant, d is the distance to the feature/environment point, and n is a constant (typically 2). Provided two observations are drawn from a normal distribution, the observations can be merged into an improved estimate by multiplying the distributions. Since the result of multiplying two Gaussian distributions is another Gaussian distribution, the operation is symmetric, associative, and can be used to combine any number of distributions in any order. The canonical form of the Gaussian distribution in n dimensions depends on the standard distributions, $\sigma_{x,y,z}$, a covariance matrix (C) and the mean (\bar{x}) [17]:

$$p(\bar{x}) = \frac{1}{(2\pi)^{n/2} \sqrt{|C|}} \exp\left(-\frac{1}{2}(\bar{x} - \bar{x}')^T C^{-1}(\bar{x} - \bar{x}')\right) \quad \text{where } C = \begin{bmatrix} \sigma_x^2 & \rho\sigma_x\sigma_y & \rho\sigma_x\sigma_z \\ \rho\sigma_x\sigma_y & \sigma_y^2 & \rho\sigma_y\sigma_z \\ \rho\sigma_x\sigma_z & \rho\sigma_y\sigma_z & \sigma_z^2 \end{bmatrix} \quad (2)$$

where the exponent is called the Mahalanobis distance. For un-correlated measured data $\rho=0$. The formulation in Equation 2 is in the spatial coordinate frame. However, all measurements are made in the camera (or sensor) coordinate frame. This problem is addressed through a transformation of parameters from the observation frame to the spatial reference frame as follows:

$$C_{\text{transformed}} = R(-\bar{\theta})^T \cdot C \cdot R(-\bar{\theta}) \quad (3)$$

where $R(\bar{\theta})$ is the rotation matrix between the two coordinate frames. The angle of the resulting principal axis can be obtained from the merged covariance matrix:

$$C_{\text{merged}} = C_1 \left(1 - \frac{C_1}{C_1 + C_2}\right) \quad (4)$$

where C_i is the covariance matrix associated with the i^{th} measurement. Additionally, a translation operation is applied to the result from Equation 2, to bring the result into the spatial reference frame.

2.4. Definition of the rating function (RF)

A rating function is used to determine the next pose of the camera from which to look at the unknown environment. The aim is to acquire new information of the environment that would lead to a more detail and more extensive

environment map. In selecting this new camera state the following four constraints are considered:

- (i) *Goal configuration is collision free*—from the probabilistic geometric environment model, (x,y,z) locations with $P_{x,y,z} < P_{\text{empty}} = 0.05$ (2σ) are considered as unoccupied. Such points form candidate configuration space camera pose coordinates.
- (ii) *Goal reached by a collision free path*—this is a function of the camera manipulator kinematics and the known environment model.
- (iii) *Goal configuration should not be far from the current one*—a Euclidean metric in configuration space, with individual weights α_i on each degree of freedom of the camera pose \bar{c} , is used to define the distance moved by the camera:

$$d = \left(\sum_{i=1}^n \alpha_i (c_i - c'_i)^2 \right)^{1/2} \quad (5)$$

where \bar{c} and \bar{c}' are vectors of the new and current camera poses respectively.

- (iv) *Measurement at the goal configuration should maximize information intake*—Specifically, the new information (NI) is equal to the expected information of the unknown/partially known region viewed from the camera pose under consideration. This is based on the known obstacles from the current environment model, the field of view of the camera (see Figure 5) and a framework for entropic thresholding of information. Shannon showed that a definition of entropy, similar in form to a corresponding definition in statistical mechanics, can be used to measure the information gained from the selection of a specific event among an ensemble of possible events [16]. This entropy function, H , can be represented as:

$$H(q_1, q_2, \dots, q_n) = - \sum_{k=1}^n q_k \ln q_k \quad (6)$$

where q_k represents the probability of occurrence for the k^{th} event, and uniquely satisfies the following three conditions [16]:

- $H(q_1, q_2, \dots, q_n)$ is a maximum for $q_k=1/n$ for $k=1 \dots n$. This implies that a uniform probability distribution possesses the maximum entropy.
- $H(AB)=H(A)+H_A(B)$ where A and B are two finite schemes. $H(AB)$ represents the total entropy of schemes A and B and $H_A(B)$ is the conditional entropy of scheme B given scheme A .
- $H(q_1, q_2, \dots, q_n, 0) = H(q_1, q_2, \dots, q_n)$ or any event with zero probability of occurrence in a scheme does not change the entropy function.

Shannon's emphasis was in describing the information content of 1-D signals. In 2-D the gray level histogram of an image can be used to define a probability distribution:

$$q_i = f_i / N \text{ for } i = 1 \dots N_{\text{gray}} \quad (7)$$

where f_i is the number of pixels in the image with gray level i , N is the total number of pixels in the image, and N_{gray} is the number of possible gray levels. With this definition, the entropy of an image for which all the q_i are

the same—corresponding to a uniform gray level distribution or maximum contrast—is a maximum. The less uniform the histogram, the lower the entropy.

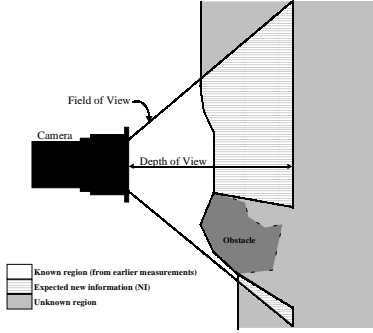


Figure 5: Evaluation of expected new information

It is possible to extend this idea of entropy to a 3-D signal—the environment model. In such an instance the scene probability distribution for entropy (information) analysis is still given by Equation 7. However, N is the maximum number of voxels visible by the vision system (limited by the depth of field and the field of view), and f_i is the number of voxels in the scene with gray level i . The possible gray values are defined as follows. For any previously sampled spatial voxel, a gray (probabilistic) occupancy value between 0 and 1 is found. Next the value, $p(\bar{x})$, is modified as follows:

$$\text{stretching : } p'(\bar{x}) = \begin{cases} \frac{1}{1-p(\bar{x})} \cdot \frac{1}{d_{\text{voxel}}} & \forall p(\bar{x}) < 0.5 \\ \frac{1}{p(\bar{x})} \cdot \frac{1}{d_{\text{voxel}}} & \forall p(\bar{x}) \geq 0.5 \end{cases} \quad (8a)$$

$$\text{scaling : } p''(\bar{x}) = \begin{cases} \frac{p'(\bar{x})-1}{2} & \forall p(\bar{x}) < 0.5 \\ 1 - \frac{p'(\bar{x})-1}{2} & \forall p(\bar{x}) \geq 0.5 \end{cases}$$

where d_{voxel} is the Euclidean distance of the voxel from the camera coordinate frame. This process causes regions with probability densities closer to 0 or 1 (regions of most certainty) to have a reduced effect on the new information expected. Regions that have a probability density closer to 0.5 (regions of least certainty of occupancy) are stretched out in the scene probability distribution, thus increasing the new expected information associated with those regions. Additionally, for all unknown/unsampled voxels a gray value between 1 and 2 is defined:

$$p(\bar{x}) = 1 + \frac{d_{\text{voxel}}}{d_{\text{max}}} \quad (8b)$$

where d_{max} is the maximum distance of any voxel in the camera field of view to the camera (equal to the depth of field). A uniform discretization of this range of gray values may be performed to define N_{gray} . With these definitions q_k (Equation 7) is evaluated and the results applied to Equation 6 resulting in a metric for new information (NI). Note that by applying the three conditions described above, this definition for NI does behave in an intuitively correct form. For example, for a given camera pose, if the field of view is occluded then NI decreases. If every point in the field of view is known and is empty then NI=0. NI increases as the number of

unknowns in the field of view increases. Further, Equation 8a results in increasing the new information expected with regions that are known with median probabilistic values i.e. values that indicate with least amount of certainty whether a voxel is occupied or not. On the other hand, regions with high probabilistic values for occupancy result in reduced associated information.

To plan the motion consistently, constraints (iii) and (iv) are merged into a unique rating function (RF):

$$\text{RF} = (NI - K \cdot d^n) \cdot (1 - P_{x,y,z}) \quad (9)$$

where K , n are scaling constants. Shorter distances exhibit a higher rating. This rating function can be evaluated and optimized to find the next most promising camera configuration from which to make future measurements of the environment. Although this choice of rating function is somewhat arbitrary, good results were obtained. Additional constraints can also be accommodated.

2.5. Suspension motion correction

A final step is to identify the motion of the camera to allow for data fusion. This process eliminates manipulator positioning errors and vehicle suspension motions. A single spatial point in the base frame, \bar{r}_i , is related to the image point (u_i, v_i) by the 4×4 transformation matrix \mathbf{g}_{01} (see Figure 6).

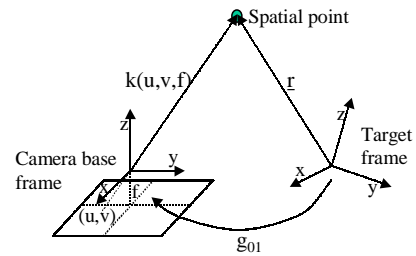


Figure 6: Relationship of camera and target frames
For motion calibration we need to identify \mathbf{g}_{01} :

$$\begin{bmatrix} k_i u_i \\ k_i v_i \\ k_i f \\ 1 \end{bmatrix} = \mathbf{g}_{01} \cdot \bar{r}_i = \begin{bmatrix} [\mathbf{R}_{01}]_{3 \times 3} & \bar{x}_{3 \times 1} \\ \bar{0} & 1 \end{bmatrix} \cdot \begin{bmatrix} r_i^x \\ r_i^y \\ r_i^z \\ 1 \end{bmatrix} \quad (10)$$

where \mathbf{R}_{01} is the rotational matrix, \bar{x} is the translation vector, f is the camera focal length, and k_i is a scaling constant. For computational reasons it is more convenient to treat the 9 rotational components of \mathbf{R}_{01} as independent (rather than a transcendental relation of 3 independent parameters). Each spatial point gives 3 algebraic equations, but also introduces a new variable, k_i —multiplicative constant to extend the i^{th} image point vector $(u, v, f)_i$ to the i^{th} spatial point in the camera coordinate frame. k_i may be found from the disparity pair of the stereo images. For n points we have:

$$\mathbf{u} = \mathbf{g}_{01} \mathbf{r} \Rightarrow \begin{bmatrix} k_1 u_1 & k_2 u_2 & \dots & k_n u_n \\ k_1 v_1 & k_2 v_2 & \dots & k_n v_n \\ k_1 f & k_2 f & \dots & k_n f \\ 1 & 1 & \dots & 1 \end{bmatrix} = \mathbf{g}_{01} \begin{bmatrix} r_1^x & r_2^x & \dots & r_n^x \\ r_1^y & r_2^y & \dots & r_n^y \\ r_1^z & r_2^z & \dots & r_n^z \\ 1 & 1 & \dots & 1 \end{bmatrix} \quad (11)$$

This set of linear equations can be readily solved using conventional techniques. A least mean square error

solution is given by:

$$\mathbf{g}_{01} = \mathbf{u}(\mathbf{r}^T \mathbf{r})^{-1} \mathbf{r}^T \quad (12)$$

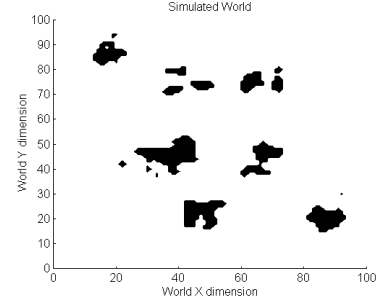
The rotation matrix, \mathbf{R}_{01} , and the translation vector, \mathbf{x} , of the camera frame with respect to the base frame are extracted directly from this solution of \mathbf{g}_{01} . However, for real measured data and associated uncertainty, a larger number of scene points are required to more correctly identify the geometric transformation matrix, \mathbf{g}_{01} . Given the $(i+1)^{\text{st}}$ scene and image point, from Equation 12 \mathbf{R}_{i+1} and \mathbf{x}_{i+1} can be obtained. A recursive method can be used to determine the mean and covariance of \mathbf{x} and \mathbf{R}_{01} based on the previous i measurements as follows:

$$\begin{aligned} \hat{\mathbf{x}}_{i+1} &= \frac{(\hat{\mathbf{x}}_i + \bar{\mathbf{x}}_{i+1})}{i+1} \\ \mathbf{C}_{i+1}^{\bar{\mathbf{x}}} &= \frac{i\mathbf{C}_i^{\bar{\mathbf{x}}} + [\bar{\mathbf{x}}_{i+1} - \hat{\mathbf{x}}_{i+1}][\bar{\mathbf{x}}_{i+1} - \hat{\mathbf{x}}_{i+1}]^T}{i+1} \\ \hat{\mathbf{R}}_{i+1}^{(l,m)} &= \frac{(\hat{\mathbf{R}}_i^{(l,m)} + \mathbf{R}_{i+1}^{(l,m)})}{i+1} \\ \mathbf{C}_{i+1}^{\mathbf{R}^{(l,m)}} &= \frac{i\mathbf{C}_i^{\mathbf{R}^{(l,m)}} + [\mathbf{R}_{i+1}^{(l,m)} - \hat{\mathbf{R}}_{i+1}^{(l,m)}][\mathbf{R}_{i+1}^{(l,m)} - \hat{\mathbf{R}}_{i+1}^{(l,m)}]^T}{i+1} \end{aligned} \quad (13)$$

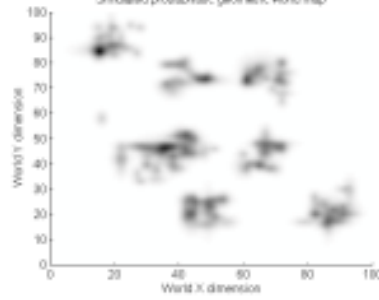
Finally, the issue of obtaining appropriate spatial points for vehicle motion compensation is addressed. Spatial points are obtained by maintaining a finite set of fiducials that are tracked during map building and visible by the cameras. As the camera moves, the fiducials move relative to the camera, eventually moving out of the camera view. This requires methods to track and identify new fiducials. First, for the purposes of this study fiducials are tracked using a computationally fast region growing method. Second, new fiducials are selected from the probabilistic environment model based on the degree of certainty with which a sampled point is known. Specifically, all local peaks in the probabilistic geometric environment map (potential fiducials) are identified. Next, at each local peak a process called spherical expansion is performed. In spherical expansion, using local gradient descent on neighboring voxels, the largest spherical region around a local peak, beyond which the voxel values increase, is found. Lastly, expanded spheres are scored based on the product of their radii and magnitude of local peak. These scores are normalized based on their distance to the current camera position. Higher scoring peaks form better fiducials and are selected accordingly. Although, alternative scoring functions may be employed, this simple one proves highly effective. Note that, by knowing the camera position and the camera arm kinematics, the robot base position can be easily extrapolated.

3. Simulation results

Results using the rating function, to explore a planar environment and develop a probabilistic geometric environment model, are given here. Figure 7 shows the results obtained of scanning a planar environment of random obstacles. Two vision systems fuse 200 samples each to give the probabilistic map seen in Figure 7(b). By increasing the number of scans taken, the uncertainty in this probabilistic map decreases.



(a) Simulated environment



(b) Probabilistic environment map after 400 scans
Figure 7: Mapping a simulated planar environment

Table 1: Comparison of explored space after 32 scans

Search method	Farthest visual point from start	Average radial distance from start	σ of viewed space
Random (m=10)	54.89	26.74	11.48
Random (m=50)	47.34	23.79	9.91
Random (m=100)	46.69	23.57	9.17
Random (m=200)	46.01	22.81	9.42
Random (m=300)	36.62	20.69	7.85
Exhaustive	34.59	19.23	7.52

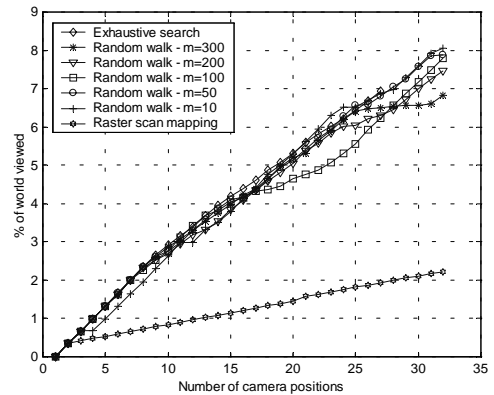


Figure 8: Percentage of environment viewed
The rating function (RF) cannot be optimized analytically. In practice, finding an optimum value for RF requires exhaustive searching through the entire known configuration space—a process that takes $O(n)$ time, where n is the number of discrete points in the configuration space. One way to reduce the search time is

to employ a finite random selection of goal configurations. For m possible configurations, this process takes $O(m)$ time— m is a constant. Thus, while the best goal configuration would be the one maximizing RF, any configuration with a high value for RF should suffice. Such a configuration can be found with reasonable effort. For comparison, results from random sample selection using 10, 50, 100, 200, and 300 points are presented along with an exhaustive search, in Figure 8 and table 1. Note that as the number of search points in the random selection increases, the explored/viewed space grows more uniformly (measured as the standard deviation of the radius of every point in the viewed environment space). This reaches a threshold as the search becomes more exhaustive in nature. Figure 8 shows the percentage increase of the environment viewed as a function of the number of scans. From this it appears that the effects of random walk searches produce equivalent results as an exhaustive search. Additionally, for comparison Figure 8 presents the results of modeling the environment using a conventional raster scan (where the next viewing position is selected sequentially from the available poses of the known environment). Clearly, there is significant decrease in performance efficiency. The specific numbers presented here are a function of camera properties (such as the FOV and the DOF) and the environment obstacles, and should be used to reflect the trend, not the exact behavior.

4. Conclusions

In field environments it is often not possible to provide robotic teams with detailed a priori environment and task models. In such unstructured environments, cooperating robots will need to create a dimensionally accurate 3-D geometric model by performing appropriate sensor actions. However, uncertainties in robot locations and sensing limitations/occlusions make this difficult. A new algorithm based on iterative sensor planning and sensor redundancy is proposed to build a geometrically consistent dimensional map of the environment for mobile robots that have articulated sensors. This algorithm is unique in that it uses a metric of the quality of information previously obtained by the sensors to find new viewing positions for the cameras. Simulations show promising results.

5. References

1. Asada, M. *Map building for a mobile robot from sensory data*. IEEE Transactions on Systems, Man, and Cybernetics. Vol. 37, no. 6, November/December 1990.
2. Baumgartner, E.T., P. S. Schenker, C. Leger, and T. L. Huntsberger. *Sensor-fused navigation and manipulation from a planetary rover*. Proceedings SPIE Symposium on Sensor Fusion and Decentralized Control in Robotic Systems, Vol. 3523, Boston, MA, Nov 1998.
3. Betge-Brezetz, S., Hebert, P., Chatila, R., and Devy, M. *Uncertain map making in natural environments*. Proceedings of the 1996 IEEE International Conference on Robotics and Automation, Minneapolis, Minnesota, April, 1996.
4. Burschka, D. Eberst, C. and Robl, C. *Vision based model generation for indoor environments*. Proceedings of the 1997

IEEE International Conference on Robotics and Automation, Albuquerque, New Mexico, April, 1997

5. Connolly, C.I. *The determination of the next best views*. Proceedings of the IEEE International Conference on Robotics and Automation, pp. 432-435, 1985.
6. Cowan, G.K. and Kovesi, P.D. *Automatic sensor placement from vision task requirements*. IEEE Transactions on Pattern Analysis and Machine Intelligence, vol. 10, no. 3, pp. 407-416, May 1988.
7. Huntsberger, T.L. *Autonomous multi-rover system for complex planetary retrieval operations*. Proceedings. SPIE Symposium on Sensor Fusion and Decentralized Control in Autonomous Robotic Agents, Pittsburgh, PA, Oct 1997, pp. 220-229.
8. Jennings, C., Murray, D., and Little, J. *Cooperative robot localization with vision-based mapping*. Proceedings of the 1999 IEEE International Conference on Robotics and Automation, Detroit, Michigan, May 1999.
9. Kecci, F., Tonko, M., Nagel, H.H., and Gengenbach, V. *Improving visually servoed disassembly operations by automatic camera placement*. Proceedings of the 1998 IEEE International Conference on Robotics and Automation, Leuven Belgium. May 1998.
10. Kruse, E., Gutsche, R., and Wahl, F.M. *Efficient, iterative, sensor based 3-D map building using rating functions in configuration space*. Proceedings of the 1996 IEEE International Conference on Robotics and Automation, Minneapolis, Minnesota, April, 1996.
11. Lumelsky, V., Mukhopadhyay, S. and Sun, K. *Sensor-based terrain acquisition: the "sightseer" strategy*. Proceedings of the 28th Conference on Decision and Control. Tampa, Florida. December 1989.
12. Luo, R.C. and M.G. Kay. *Multisensor integration and fusion in intelligent systems*. IEEE Transactions on Systems, Man, and Cybernetics, Vol. 19, No. 5, September, 1989.
13. Rekleitis, I., Dudek, G., and Milios, E. *Multi-robot collaboration for robust exploration*. Proceedings of the 2000 IEEE International Conference on Robotics and Automation, San Francisco, CA. April, 2000.
14. Repo, T. and Roning, J. *Modeling structured environments by a single moving camera*. Proceedings. Second International Conference on 3-D Digital Imaging and Modeling, 1999. On page(s): 340 - 347, 4-8 Oct. 1999
15. Shaffer, G.; Stentz, A. *A robotic system for underground coal mining*. Proceedings of the IEEE International Conference on Robotics and Automation, 1992. Pages(s): 633 -638 vol.1
16. Shannon, C. E. *A mathematical theory of communication*. The Bell System Technical Journal, vol. 27, pp. 379-423 and 623-656, July and October, 1948.
17. Smith, R.C. and Cheeseman, P. *On the representation and estimation of spatial uncertainty*. International Journal of Robotics Research. 5(4): 56-68
18. Tarabanis, K.A., Allen, P.K. and Tsai, R.Y. *A survey of sensor planning in computer vision*. IEEE Transactions on Robotics and Automation, Vol. 11 no. 1, Pp. 86-104. February, 1995.
19. Thrun, S., Burgard, W., and Fox, D. *A real-time algorithm for mobile robot mapping with applications to multi-robot and 3D mapping*. Proceedings of the 2000 IEEE International Conference on Robotics and Automation. San Francisco, CA, April, 2000.
20. Sujan, V.A. *Compensating for Uncertainty in the Control of Cooperative Robots in Field Environments*. Ph.D. Thesis, Department of Mechanical Engineering, Massachusetts Institute of Technology, June 2002.

Lightweight Hyper-redundant Binary Elements for Planetary Exploration Robots

Vivek A. Sujan, Matthew D. Lichter and Steven Dubowsky
Department of Mechanical Engineering
Massachusetts Institute of Technology
Cambridge, MA 02139

Abstract—This paper presents the design of a new lightweight, hyper-redundant, deployable Binary Robotic Articulated Intelligent Device (BRAID), for space robotic systems. The BRAID element is intended to meet the challenges of future space robotic systems that need to perform more complex tasks than are currently feasible. It is lightweight, has a high degree of freedom and a large workspace. The device is based on embedded muscle type binary actuators and flexure linkages. Such a system may be used for a wide range of tasks, and requires minimal control computation and power resources.

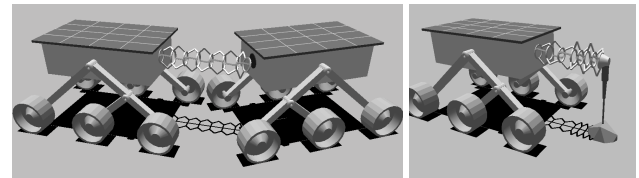
Index terms—Binary robot, hyper-redundant, polymer actuator

I. INTRODUCTION

Future missions to explore Mars will require robots to perform complex tasks such as scouting, mining, conducting science experiments, and constructing facilities, for human explorers and settlers [13]. To accomplish these objectives, future planetary robotic systems will need to work faster, travel larger distances, perform highly complex operations, and work with a higher degree of autonomy than today's technology would permit. New design concepts are required to meet these challenges. For example, robots will require devices for deploying communication antennas, rapid positioning of scientific sensors and facilitating assembly [13]. A single, yet lightweight and simple device that could perform a number of these tasks would be highly desirable. It would need to have fine motion resolution, a large motion workspace, multiple degrees of freedom, control simplicity, and have a small stowed volume.

This paper presents the design of an element that is intended to meet these requirements. This device, called a Binary Robotic Articulated Intelligent Device (BRAID), consists of compliant mechanisms with large numbers of embedded actuators. Figure 1 shows two potential application concepts of the BRAID element. In some ways it resembles deployable systems that have been used in the past for such space applications as: deployable booms, solar arrays, antennas, articulated masts and others [4, 7, 18, 22]. These devices can be deployed from a small package into

relatively large structures. However, in general these structures are not controllable in terms of being able to assume different commanded configurations. Once deployed they are usually not retractable. They are also usually constructed from heavy and complex components, such as gears, motors, cables, etc., although there are some notable exceptions [3, 20].



(a) mating two rovers (b) coring rock samples
Figure 1. Two BRAID robotic potential applications

In the robotic research community, efforts have been made to develop concepts of simple manipulators with good performance. An interesting example is binary manipulators [5, 12, 15]. In this concept, a manipulator is controlled by activating the actuators that can assume only one of two states (“on” or “off”). The joint level control is very simple. By simply activating the given actuator in the system a discrete change in state is obtained. Often, the control does not require feedback sensors. The two states are the extreme positions of the actuator. Examples include pistons, solenoids or motors. This form of control has been classified as sensor-less manipulation [6, 10, 15].

As the number of binary actuators in the system increases, the capabilities of the device approaches that of a conventional continuous manipulator. This is analogous to the revolution of the digital computer replacing the analog computer. However, this leads to mechanisms with complex system kinematics. Studies of the kinematics and control of such “hyper-redundant” manipulators, both with and without binary actuation have been performed [2, 5, 11, 12, 14].

This paper presents the design of a new lightweight, hyper-redundant, deployable Binary Robotic Articulated Intelligent Device (BRAID) for space robotic systems. The BRAID element is made of a serial chain of parallel stages (see Figure 2). Each three DOF stage has three flexure-

based legs, each with muscle type binary actuators. In the experimental system described in this paper these are shape memory alloy (SMA) actuators. As discussed later, more promising polymer actuators are now being implemented in this study. Muscle actuation allows binary operation of each leg. The flexures are simple and light weight. This type of structure could be used in space robotics as an instrument positioning device, a highly articulated manipulator, a deployable boom (for solar arrays and antennas), etc. The experimental BRAID built consists of five parallel stages, yielding 15 binary degrees of freedom. Thus it has 2^{15} (32,768) discrete configurations. Thus, the system can approximate a continuous system in dexterity and utility. By its polymer construction and binary actuation the design is very lightweight and simple, appropriate for space exploration systems.

This paper is divided as follows: Section 2 describes the parallel link stage design of the BRAID element. Section 3 presents a discussion of its actuators and the actuator control. Section 4 explains the forward kinematics of the BRAID. Section 5 presents two approaches for solving its inverse kinematics.

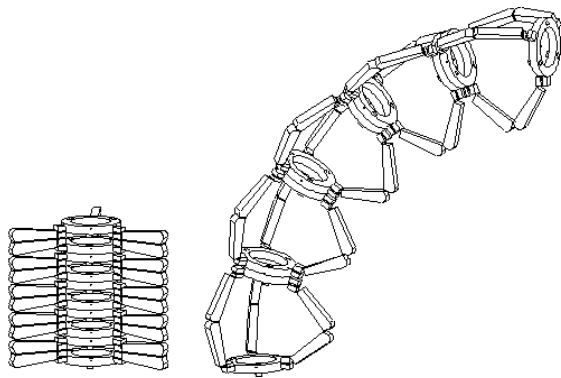
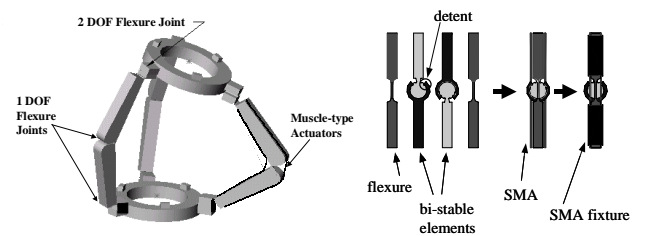


Figure 2: Basic design of the BRAID element

II. MANIPULATOR PARALLEL LINK STAGE DESIGN

Figure 3(a) shows one stage of the BRAID element. Each parallel link stage has three legs and actuators. Each leg has three flexure joints—two one DOF joints and one two DOF joint. This results in four non-intersecting axes per leg: three in parallel and a fourth orthogonal to the first three. Coupling the three legs together (symmetrically 120° apart) gives the parallel link stage three DOF mobility (vertical translation, pitch, and yaw). If each leg has only one actuator (an SMA wire in tension) the restoration force to change the binary states is provided by the elastic flexure joints. A pair of antagonistic actuators does not require the elastic effect. Detents help lock each binary leg into a discrete state (see Figure 3(b)) and provide more accurate and repeatable positioning. They also eliminate the need for power while the BRAID is stationary.



(a) parallel link stage (b) detent based binary joint

Figure 3: Parallel link stage of BRAID

The concept of using flexures to replace hinges and bearings is not new. Short plastic hinges can commonly be seen in commercial applications such as cabinet doors, tool box lids, shampoo bottle caps, etc. Their design requires careful attention to their structure mechanics. In the BRAID application large range of motions and low stiffnesses are desired, and fatigue strength proves to be critical. Repeated bending of a flexure can cause fatigue failure. The relationship between performance and fatigue life can be seen by considering a simple beam of thickness t , with Young's modulus E , bent elastically to a radius of R . The surface strain and maximum elastic stress is given by:

$$\epsilon = \frac{t}{2R} \quad \text{and} \quad \sigma = E \frac{t}{2R} \quad (1)$$

This stress must not exceed the fatigue yield strength of the material, σ_f . Hence, the minimum bend radius is given by:

$$R \geq \frac{t}{2} \left(\frac{E}{\sigma_f} \right) = \frac{t}{2} \left(\frac{1}{M} \right) \quad (2)$$

Materials that can be bent to the smallest radius or the ones where M (defined in Equation 2) is maximized are desirable because they give the largest range of motion. Literature suggests the best choices are polymeric materials and elastomers with M equal to 3×10^{-2} [1]. Materials such as polyethylene, polypropylene and nylon fall into this category. For comparison, for spring steel M equals 0.5×10^{-2} (which would be appropriate when high stiffness and small range of motion is desired). An ultra high molecular weight polyethylene was chosen here, based on its machinability, fatigue life, stiffness, weight, and cost.

The experimental system constructed is shown in Figure 4. It consists of five parallel link stages coupled serially, giving a 5 DOF end-effector. This device has yet to have its detents installed. With binary control this structure has $2^{3 \times 5}$ (or 32768) possible states giving the device suitable freedom for a number of applications. For other applications this could be extended to 10 or 20 stages giving $2^{3 \times 20}$ (approximately 10^{18}) possible states. While this closely approximates a continuous workspace, it leads to some interesting inverse kinematic problems due to the hyper-redundancy of the system, see Section 5.

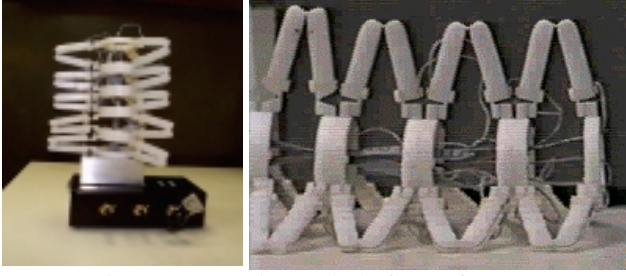


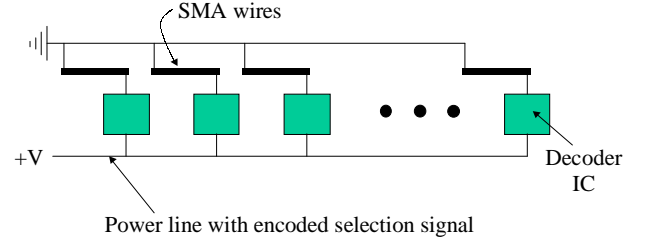
Figure 4: Experimental platform of BRAID

III. ACTUATOR AND ACTUATOR CONTROL

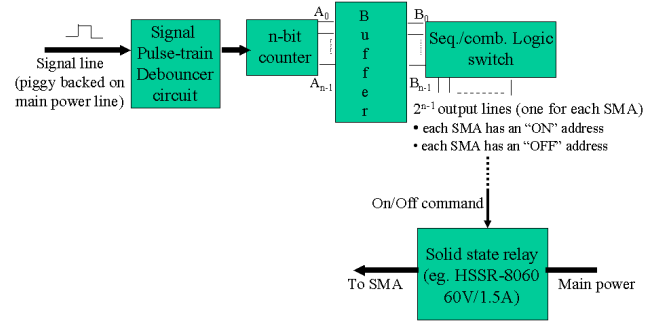
For some applications, a hyper-redundant BRAID would need a large number of actuators. The actuators are assumed to be polymer-based smart materials. These materials include conducting polymers and electrostrictive polymers [17, 21]. However, while these materials are anticipated to meet the needs of the concept in the future, they have not yet reached a sufficient state of development to perform practical experimental demonstrations in devices today. In the near term, shape memory alloys (SMAs) are being used for the muscle actuators. SMAs are a class of alloys which are able to remember their shape and are able to return to that shape after being deformed, given a certain temperature change [8]. These alloys can be used as actuators, as the ratio of the deformation stress to the actuated recovery stress can be higher than 10 to 1. It is proposed that each link be actuated by a pair of antagonistic SMA wires, which open and close the link. Appropriate wire length and thickness are easily determined based on the range of motion and the force output desired. For this laboratory demonstration, the payload is assumed to be a sensor such as a CCD camera weighing less than 50 grams. The stiffness of the antagonistic pair and the flexures must also be accounted for. However, the design of the SMA actuators is not a serious challenge.

To actuate the BRAID element, the actuators need to be triggered selectively, as required by the inverse kinematics. Conceptually, such a binary control is simple requiring no sensor feedback. However, the large number of actuators can rapidly make the physical realization of such a system difficult, if each actuator requires unique power supply lines. A multitude of wiring introduces possibility for error and would result in additional weight and volume, large external forces, and complexity. The BRAID concept uses a more compact and efficient form of supplying power and control (see Figure 5). A common power line and ground are provided to all the actuators. Each actuator has a small “decoder” chip that can be triggered into either binary state by a carrier signal “piggybacked” on the power line. The carrier signal is a sequence of pulses that identifies a unique address in the form of a binary word for the actuator that requires toggling. This architecture reduces the wiring of the entire system to only two wires (see Figure 5). This can easily be implemented in the form of conducting paint/tape

(on the non-conducting polyethylene substrate). This bus architecture is currently being implemented.



(a) Overview of actuator control electronics



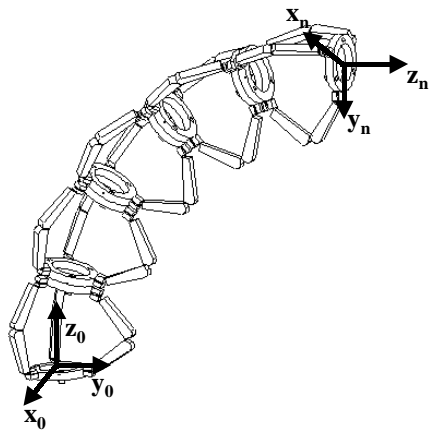
(b) Power/Control Bus Decoder Architecture

Figure 5: SMA Power and Control Bus

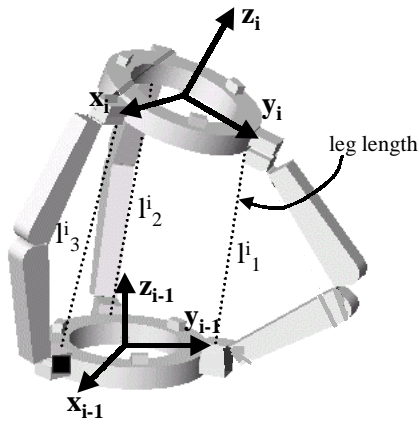
IV. FORWARD KINEMATICS

Binary devices present a number of challenges not found in conventional continuous systems. For example, a continuous robot can reach an infinite number of points within its workspace while a binary robot can only reach a finite number of points. A binary robot’s workspace is thus a discrete point cloud. A BRAID based system adds further challenges, due to the complexity of its kinematics. A typical four by four homogeneous transformation matrix is formulated as a combination of a rotation matrix and a translation vector of one coordinate frame with respect to another. The kinematic variables are then three rotational and three translational variables (six DOF). In a single parallel link stage of the BRAID system, the three legs are positioned about the vertices of two equilateral triangles. Additionally, based on the joint configuration of each leg, the single stage has only three degrees of freedom—pitch and yaw rotations and a vertical translation. In general, given the four by four transformation matrix $A_{i-1,i}$, of the i^{th} coordinate frame with respect to the $i-1^{\text{th}}$ coordinate frame (see Figure 6(b)), one can derive the forward kinematics of the entire n -staged system. A_{0n} defines the forward kinematics from base to end-effector of the entire system and is simply given by:

$$A_{0n} = A_{0,1}A_{1,2}A_{2,3} \cdots A_{n-1,n} = \prod_{i=1}^n A_{i-1,i} \quad (3)$$



(a) BRAID system frames



(b) i^{th} parallel link stage

Figure 6: Critical parameter representation of BRAID system

In this formulation the leg lengths (see Figure 6) are the control variables. The relationship between these leg lengths and the pitch, yaw, and vertical translation of the i^{th} coordinate frame with respect to the $i-1^{\text{th}}$ coordinate frame (see Figure 6) can be formulated. This relationship does not have a closed form solution. Hence, $A_{i-1,i}$ is only a function of the variable leg lengths of the i^{th} stage ($l_{1,2,3}^i$). Since every leg in the system can be in only one of two states (binary), each leg length can have only one of two values (defined as l_{\min} and l_{\max}). Hence, each term of $A_{i-1,i}$ can have only 8 different discrete values.

Figure 7 shows the workspace generated for a 5 stage BRAID element. The workspace for this example consists of 2^{15} unique states. However, the workspace is clearly non-uniform in its distribution. Optimization of this workspace in terms of density of reachable states is an area of continuing research.

Workspace of 5 stage BRAID system

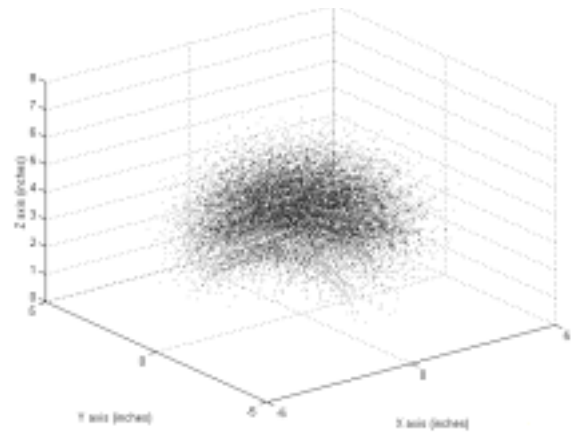


Figure 7: Workspace of 5 stage BRIAD element (BRAID element base center=origin)

V. INVERSE KINEMATICS

Once the forward kinematics of the system have been developed, the problem of executing practical tasks requires the solution to the inverse kinematics problem. While the hardware costs and control complexity of a binary manipulator are lower than those of a continuously-actuated manipulator, there is a tradeoff in the complexity of the trajectory planning and inverse kinematics software. As expected, the inverse kinematics problem cannot be expressed in a closed form solution. Brute force or exhaustive search methods may prove appealing for systems with few stages (less than 5), but become impractical for larger systems. As the number of degrees of freedom increase, the complexity of the workspace grows exponentially. For every additional stage there is about an order of magnitude increase in the number of states in the workspace. Hence, for large systems more efficient search methods are required to find “optimum” solutions. This section presents two possible search methods for the inverse kinematics problem. The first is a genetic search algorithm and the second is a combinatorial heuristic search algorithm. The search metric for both algorithms is to minimize the distance between the end-effector and desired position. Both algorithms will be briefly described and their results will be presented.

A. Genetic Search Algorithm

Here a classical genetic algorithm approach for finding an optimum solution is used, where each generation consists of m -bit binary words describing the manipulator state (where m is the number of actuators). A full description of genetic algorithms can be found in [9].

B. Combinatorial Heuristic Search Algorithm

This algorithm was first described in [15]. In order to avoid exponential growth of the search space as the number of actuators grow, the inverse kinematics are solved by changing the state of only a few actuators at any given time. This is perceived as a k -bit change to the given system state, where any system state is defined by an m -bit word (m is the number of actuators). At any state all possible changes (up to k -bits, where $k \leq m$) are evaluated to determine the one that optimizes the search metric (i.e. reduces the error between the end-effector position and the desired position). This optimal change forms the new state of the system and the search procedure repeats until convergence. This search method reduces the computational complexity from $O(2^m)$ to $O(m^k)$ or from exponential computational time to polynomial computational time. This is seen through the following observation. For the binary robot being considered with m actuators, moving towards its target by changing up to k -bits requires a search through $\binom{m}{0} + \binom{m}{1} + \dots + \binom{m}{k}$ possible states, where $\binom{m}{k} = \frac{m!}{k!(m-k)!}$. Expanding these terms, the highest power of m is found to be k . An exhaustive search of same system would require exactly 2^m search states.

C. Search Algorithm Results

Figure 8 shows the performance of the BRAID with different number of stages (n), using the genetic search algorithm, attempting to reach a desired position from an initial position. The actuated leg length was normalized to one inch. Figure 8 shows that, the steady state error decreases with increasing n . Note that the absolute error difference (after convergence) for 12 stages and 17 stages is 0.015 inches. Thus, although the number of reachable points increases with the number of stages, the accuracy to reach a given point might not increase. As expected of a genetic algorithm, the average error across a given population decreases with increasing generation.

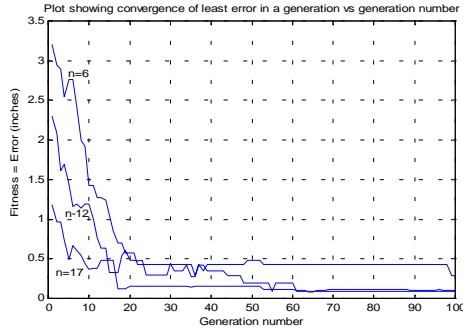


Figure 8: Results of genetic search algorithm for n -staged BRIAD element (population size = 30, probability of crossover = 0.6, probability of bit-wise mutation = 0.02)

Figure 9 shows the performance of the combinatorial heuristic search algorithm, attempting to reach a desired position from an initial position. The algorithm was tested

on the BRAID, with variable number of stages. Again, the actuated link length was normalized to one inch. At every search step, a search through $\binom{m}{0} + \binom{m}{1} + \dots + \binom{m}{k}$ states

was performed (where $k=3$), giving a new end-effector position with less error. From figure 9, it is seen that the error convergence rate stays fairly constant with increasing system complexity (increasing n , the number of parallel link stages). However, each step needs more computation as $\binom{m}{0} + \binom{m}{1} + \dots + \binom{m}{k}$ increases with increasing n .

Additionally, in general the steady state error decreases with the increasing n . This is expected intuitively since there are more finite solutions in the workspace. Note again, that the absolute error difference (after convergence) for 10 stages and 12 stages is 0.019 inches. Thus, although the number of reachable points increases with the number of stages, the accuracy to reach a given point might not increase

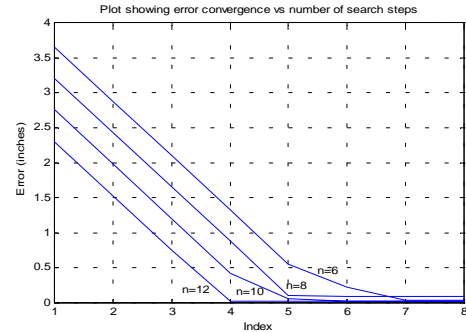


Figure 9: Results of combinatorial heuristic search algorithm for n -staged BRAID element (maximum allowable bit changes = 3)

VI. CONCLUSIONS

A new lightweight hyper-redundant binary device with potential application to space robotics systems has been presented. Such a system may be used for the deployment of booms and antennas, rapid and accurate positioning of sensors, and manipulation requiring simple and highly articulated onboard manipulators, all while maintaining a small stowed volume. This device is comprised of a serial chain of parallel stages and can collapse to a small stowed volume. Each stage is composed of three flexure-based elements, each with muscle type actuators, permitting only binary operation of each link. Each parallel link stage has 3 DOF. By coupling these parallel stages in series, a 5 DOF end-effector pose is obtained. With a large number of actuators, this system can approximate a continuous system in dexterity and utility. In such a system, only a binary word command signal is needed to control the motion of the entire system. Controller feedback and the corresponding computational load is completely eliminated. Further, the system power bus structure can be implemented so as to eliminate the need for individual power wires to the large array of actuators. This scheme eliminates all but one power and one ground line in the system. The system does

not have a closed form solution of its forward kinematics. Numerical solutions to the BRAID inverse kinematics problem (or trajectory planning), are also presented. These search techniques were based on a genetic algorithm and a combinatorial heuristic algorithm. Both methods prove to be highly efficient as compared to exhaustive search methods. The workspace of such manipulators and the actuator triggering sequence are areas of current study. Such optimizations would allow for better distributed workspaces, allowing good dexterity throughout a region. Preliminary experimental results show good promise [16]. A detailed discussion of these results are beyond the scope of this paper.

VII. ACKNOWLEDGEMENTS

The authors would like to acknowledge the NASA Institute of Advance Concepts (NIAC) for their support in this work. Also the contributions of Guillermo Oropeza (MIT) in fabrication of the experimental BRAID is acknowledged [19].

VIII. REFERENCES

- [1] Ashby, M. *Material selection in mechanical design*. Butterworth-Heinemann, Oxford, 1992.
- [2] Chirikjian, G.S.; Burdick, J.W. *The kinematics of hyper-redundant robot locomotion*. IEEE Transactions on Robotics and Automation. Volume: 11 Issue: 6, Dec. 1995 Page(s): 781 -793
- [3] Darby, A. P. and Pellegrino, S. *Modeling and control of a flexible structure incorporating inertial stick-slip actuators*. Journal of Guidance, Control, and Dynamics, 22, 36-43, 1999.
- [4] Dotson RD. *Spacecraft deployable structure testing*. Space Systems Design and Development Testing (AGARD-CP-561). AGARD. 1995, pp.6/1-12. Neuilly sur Seine, France.
- [5] Ebert-Uphoff, I.; Chirikjian, G.S. *Inverse kinematics of discretely actuated hyper-redundant manipulators using workspace densities*. Proceedings of the IEEE International Conference on Robotics and Automation, 1996, Volume: 1, Page(s): 139 -145 vol.1.
- [6] Erdmann, M.A. and Mason, M.T. *Exploration of sensor-less manipulation*. IEEE Journal of Robotics and Automation, Vol. 4, pp 369-379, August 1988.
- [7] Gantes, C., Connor, J., and Logcher, R.D. *Structural analysis and design of deployable structures*. Computers and Structures. Vol. 32, No. 3/4, pp. 661-669, 1989.
- [8] Gilbertson, R. *Muscle wires*. San Alsamo, CA 1994.
- [9] Goldberg, D. *Genetic Algorithms in Search, Optimization, and Machine Learning*. Addison-Wesley, Reading, MA 1989
- [10] Goldberg, K. *Orienting polygonal parts without sensors*. Algorithmica, 1992, Special Robotics Issue.
- [11] Huang, M.Z.; Shou-Hung Ling *Kinematics of a class of hybrid robotic mechanisms with parallel and series modules* Proceedings of the 1994 IEEE International Conference on Robotics and Automation, Page(s): 2180 -2185 vol.3
- [12] Hughes, P.C. *Trussarm – a variable geometry truss manipulator*. Journal of intelligent materials, systems and structures, vol. 2, pp. 148-160, April '91.
- [13] Huntsberger, T.L., G. Rodriguez, and P. S. Schenker. *Robotics: challenges for robotic and human Mars exploration*. Proceedings of ROBOTICS2000, Albuquerque, NM, Mar 2000.
- [14] Kwon, S; Youngil Youm *General algorithm for automatic generation of the workspace for n-link redundant manipulators*. Proceedings of the International Conference Advanced Robotics, 1991. 'Robots in Unstructured Environments', Page(s): 1722 -1725 vol.2
- [15] Lees, D.S. and Chirikjian, G.S. *A combinatorial approach to trajectory planning for binary manipulators*. Proceedings of the IEEE International Conference on Robotics and Automation, Minneapolis, Minnesota, April 1996.
- [16] Lichter, M.D., Sujun, V.A., Dubowsky, S. *Experimental Demonstration of a New Design Paradigm in Space Robotics*. Proceedings of the Seventh International Symposium on Experimental Robotics, ISER 00. Dec 10-13, 2000, Honolulu, Hawaii.
- [17] Madden J D, Cush R A, Kanigan T S, et al. *Fast-contracting Polypyrrole Actuators*. *Synthetic Metals*, 113: 185-193, 2000
- [18] Meguro A, Mitsugi J, Ando K. *A modular cable-mesh deployable structure for large scale satellite communication antennas*. Transactions of the Institute of Electronics, Information & Communication Engineers B-II, vol.J76B-II, no.5, May 1993, pp.476-84. Japan.
- [19] Oropeza, G. *The Design of Lightweight Deployable Structures for Space Applications*. Thesis for the Bachelors of Science in Mechanical Engineering, Massachusetts Institute of Technology, May 1999.
- [20] Pellegrino, S. and Guest, S. D. *Deployable Structures: Theory and Applications*. Proceedings of IUTAM-IASS Symposium held in Cambridge, September 1998, Kluwer Academic Publishers, Dordrecht
- [21] Pelrine R, Kornbluh R, Pei Q, et al. *High-speed Electrically Actuated Elastomers with Over 100% Strain*. *Science*, Vol. 287, No. 5454, 836-839, 2000.
- [22] Syromiatnikov, V.S. *Manipulator system for module re docking on the Mir Orbital Complex*. Proceedings of the 1992 IEEE International Conference on Robotics and Automation, 1992 Page(s): 913 -918 vol.1

Hyper-Redundant Robot Manipulators Actuated by Optimized Binary Dielectric Polymers

Andreas Wingert*, Matthew Lichter**, Steven Dubowsky, Moustapha Hafez
Department of Mechanical Engineering, Massachusetts Institute of Technology,
Cambridge, MA 02139 USA

ABSTRACT

This paper reports on the development of a lightweight hyper-redundant manipulator driven by embedded dielectric polymer actuators. This manipulator uses binary actuation and belongs to a class of digital mechanisms that are able to perform precise discrete motions without the need for sensing and feedback control. The system is built from an assembly of modular parallel stages and has potential to be miniaturized for applications ranging from biomedical devices to space system components. The polymer actuators can make such devices feasible. This paper presents the design of a modular polymer actuator that can work under both tension and compression. The actuators achieve improved performance by incorporating an elastic passive element to maintain uniform force-displacement characteristic and bi-stable action. A flexible frame also insures nearly optimal pre-strain required by dielectric film based actuators.

Keywords: dielectric, elastomer, polymer actuator, parallel mechanism, binary, bi-stable, hyper-redundant, embedded actuation

1 INTRODUCTION

Proposed tasks for future robotic systems, ranging from space exploration to medical devices, will require robotic devices and components that are simple, robust, lightweight, inexpensive, and easy to control. Hyper-redundant binary systems have been proposed to meet this need^{1,2}. It has been shown that performance of a binary robotic system approaches that of a continuous system, as the number of DOF increases³. However, high DOF systems are not feasible with conventional components⁴. A major limitation is the actuator technology. In recent years, important progress has been made in the area of dielectric polymer actuators. Analysis suggests that dielectric polymer actuators have the potential of overcoming limitations of conventional actuators and serving as a key component for high DOF binary manipulators.

Under laboratory conditions, dielectric polymer actuators have achieved very high energy densities, exceeding those of conventional technologies such as electromagnets⁵. To date, the performance of these actuators when applied to practical devices is less than what can be achieved under ideal laboratory conditions⁶.

Here a design for a high DOF binary manipulator driven by modular dielectric polymer based actuators is presented. The actuator consists of an integrated module consisting of the polymer film, an elastic frame and a passive elastic element. The actuator module applies boundary conditions that enhance the performance of dielectric polymers. This actuator module can work under both tension and compression and has a constant force through its stroke. It can be implemented into mechanical systems without the need of external restoring forces. The actuator module is used to power a robotic element called a Binary Robotic Articulated Intelligent Device (BRAID), shown in Figure 1. The BRAID is a lightweight, hyper-redundant binary manipulator with a large number of embedded actuators⁷. The prototype demonstrates feasibility of the modular dielectric polymer actuators.

* arw@mit.edu; **lichter@mit.edu; phone 617 253-2334; http://robots.mit.edu; Field and Space Robotics Laboratory, Massachusetts Institute of Technology, Rm. 3-473m, 77 Massachusetts Ave., Cambridge, MA 02139

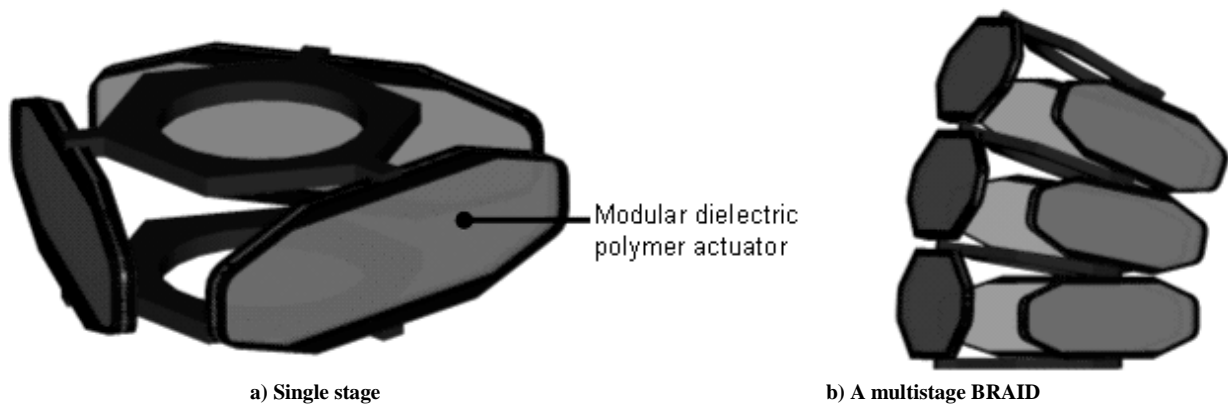


Figure 1. Representation of a dielectric polymer actuated BRAID

2 BACKGROUND AND LITERATURE

The operating principle of a dielectric polymer actuator is simple and shown in Figure 2. An elastomeric film is coated on both sides with compliant electrodes. As a voltage is applied across the electrodes, electrostatic forces will cause the film to compress in thickness and expand in area^{8,9}. This area expansion can be used to actuate mechanical systems. The individual films can be layered to increase actuation forces.

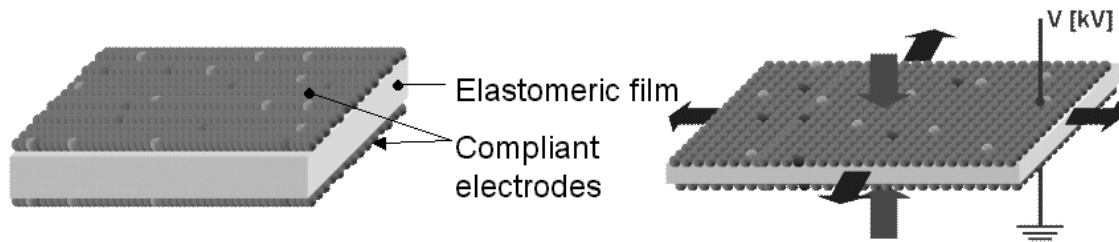


Figure 2. Dielectric polymer actuator operating principle

Dielectric polymers have been proposed for use in linear actuators, loudspeakers, solid state optical devices, and as generators^{5,10}. A variety of geometric configurations convert the area expansion of the film to linear motion. For example, the actuator film can be constrained in planar frames or be rolled into tubes that change length⁵. For these cases, the direction of the actuator motion is in the same plane as the film expansion. An example of an out-of-plane device is a cone-shaped actuator, in which the motion is normal to the undeformed film¹¹.

Planar geometries of dielectric polymer actuators have been proposed to power a snake-like manipulator and an insect-inspired hexapedal walker^{5,12}. A conical geometry has been proposed to power an inchworm robot¹¹. Since the actuators only work in tension, some external restoring force is required, which can be achieved in a variety of ways. For the case of the snake-like manipulator, each degree of freedom is controlled by an antagonistic pair of actuators. The hexapedal walker and the inchworm robot use return springs to provide the restoring force^{11,12}.

For the actuator proposed here, the restoring force is provided by a flexible frame that is directly bonded to the film, resulting in a compact structural module with embedded actuation.

A promising dielectric polymer is VHBTM 4910 made by 3MTM and sold as an adhesive tape. This is a very elastic material and has been shown to produce the greatest strains and energy densities in laboratory demonstrations. Up to 380% strain has been reported⁵. However, such high strains have not been reported for actuators when the material is used in practical applications. This is due to the fact that in applications the boundary conditions that maximize performance are not maintained. The modular actuator concept presented in this paper is intended to eliminate this problem.

3 EMBEDDED ACTUATOR DESIGN

3.1 Operating principle

The dielectric polymer that separates the electrodes experiences an electrostatic pressure as a charge is applied to the electrodes. If both the dielectric material and the electrodes are compliant, then the effective pressure is given by

$$p = \epsilon \epsilon_0 E^2 = \epsilon \epsilon_0 \left(\frac{V}{z} \right)^2 \quad (1)$$

where ϵ is the relative dielectric constant, ϵ_0 is the permittivity of free space, and E is the applied electric field, which is the ratio of the applied voltage (V) over the film thickness (z)^{8,9,13}. In general, the larger the effective pressure, the larger the actuator strain obtained.

Understanding the implication of this equation is useful in actuator design. Equation 1 suggests that a high effective pressure will result from a large electric field. The maximum electric field that can be applied to the film without damaging it is the electric breakdown field. The breakdown field for VHBTM 4910 increases by more than an order of magnitude with pre-stretching¹⁴. Since the electric field term (E) in Equation 1 is squared, pre-stretching this material can increase the maximum attainable effective pressure by two orders of magnitude. To fully exploit the potential of dielectric polymer actuators, the pre-stretching boundary conditions on the film are very important. The amount of pre-stretching of the film also affects the dielectric constant, however its variance with pre-strain is small and therefore believed to be less significant in actuator development¹⁴.

3.2 Flexible Frames

A simple way to produce linear motion with dielectric polymers is to stretch the actuator film between two parallel beams, as shown in Figure 3. As a voltage is applied to the electrodes, the film expands in area and allows the beams to separate if they are pre-loaded. Since the electric breakdown field increases with pre-stretching, such an implementation works best if the film is stretched in both planar directions. The pre-stretching also reduces the thickness of the film, which in turn reduces the voltage to achieve a given electric field.

In this implementation, the vertical sides of the film are free, allowing the film to bow in. From Figure 3 it is evident that the amount of pre-stretching in the passive direction is not uniform throughout the actuator film. Since the film is largely incompressible (constant volume), it is thin close to the beams and thicker at the center. Applying an electric potential across the electrodes creates a non-uniform pressure and deformation of the film. Thus, not all areas of the film are actuated fully. Since the film is not constrained in the passive directions, it exhibits some motion in that direction upon actuation. This motion does not produce useful mechanical work. The challenge is to maintain the pre-stretched boundary conditions on the film without interfering with the desired motion of the actuator. One way to ensure uniformity in the film would be to increase the aspect ratio of the actuator by increasing the width (x) and reducing the height (y). However, such geometry would be inappropriate for many applications.

To solve this problem the film can be incorporated into a flexible frame, as shown in Figure 3b. The frame consists of two parallel beams that are connected with flexible links. The frame geometry is designed such that all areas of film undergo approximately equal expansion under actuation. The frame is a monolithic piece of Delrin[®]. Flexibility is provided by reducing the wall thickness in certain areas. The acrylic film is placed between two such frames.

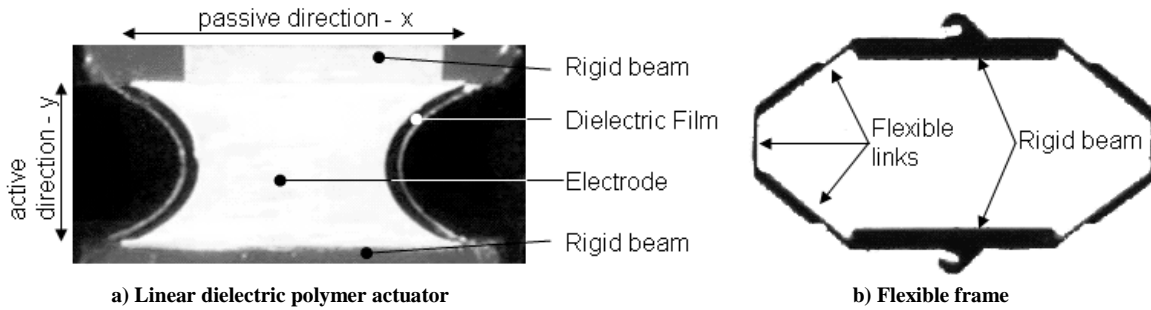


Figure 3. Methods of implementing dielectric polymer actuators

A second key function of the frame is that it provides an elastic restoring force that permits the actuator to work under both tension and compression. A welcome side-effect of the frame is that the risk of tearing of the film at its exposed edges is greatly reduced. The frame also prevents current arcs from developing around the edges of the film.

Figure 4a shows an exploded view of the actuator module with the dielectric film integrated into its flexible frame. Higher actuation forces can be achieved by increasing the number of layers of film sandwiched between the frames. When using an even number of dielectric films, the electrodes can be arranged so that the two outer electrodes are both grounded. The high voltage is only present in the inside of the actuator and is thus shielded from the environment. The actuator discussed here uses two layers of the dielectric polymer as shown in Figure 4.

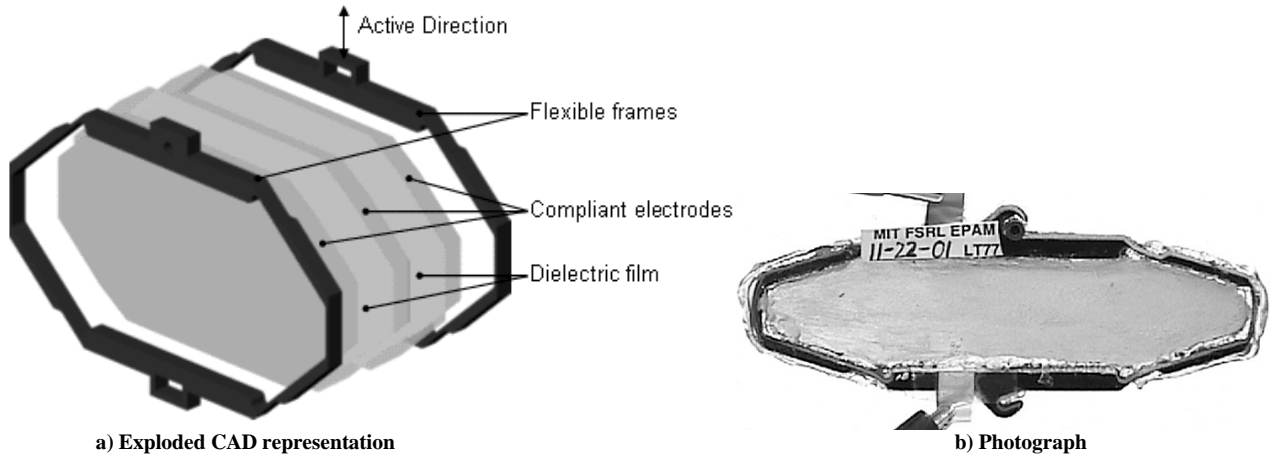


Figure 4. Embedded flexible-frame actuator module

3.3 Actuator performance and physical actuator model

To evaluate the performance of the actuator, the force-displacement characteristics were measured, see Figure 5. Curves are shown for an actuator at 0kV, 5.5kV, and completing a work cycle. The work cycle is generated by constraining the displacement of the actuator. A voltage of 5.5kV is applied and the force applied to the constraint is recorded. While keeping the voltage fixed, the constraint is moved until the actuator force is zero. The voltage is then removed and the process is repeated. The area enclosed by a counter-clockwise work cycle corresponds to the work output per cycle⁶.

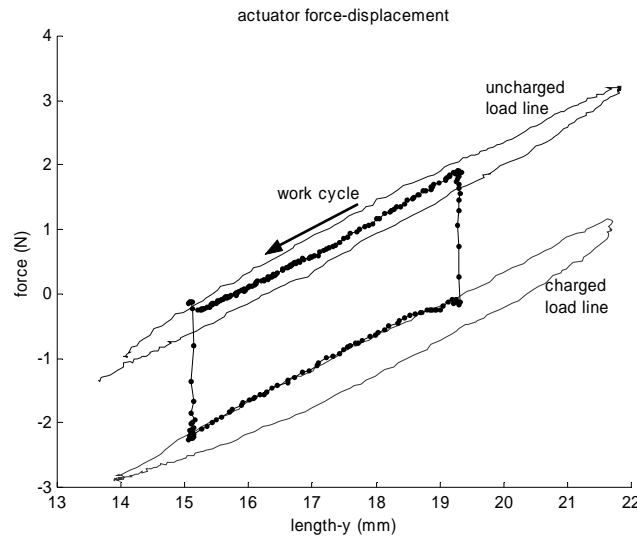


Figure 5. Actuator stiffness and work cycle

The slope of the curve, which corresponds to the stiffness of the actuator, is nearly constant at 0.5N/mm for the range shown. Some hysteresis is evident, which is attributed to the viscoelastic losses of the film and frame⁹. As shown in Figure 5, changing the voltage from 0 to 5.5kV offsets the curve, but does not significantly change its slope, suggesting that the stiffness of the actuator is independent of the state of actuation over the range shown. The actuator can therefore be modeled as a spring that changes its undeformed length upon actuation while maintaining its stiffness, as shown in Figure 6a. The corresponding force-displacement curves are shown in Figure 6b.

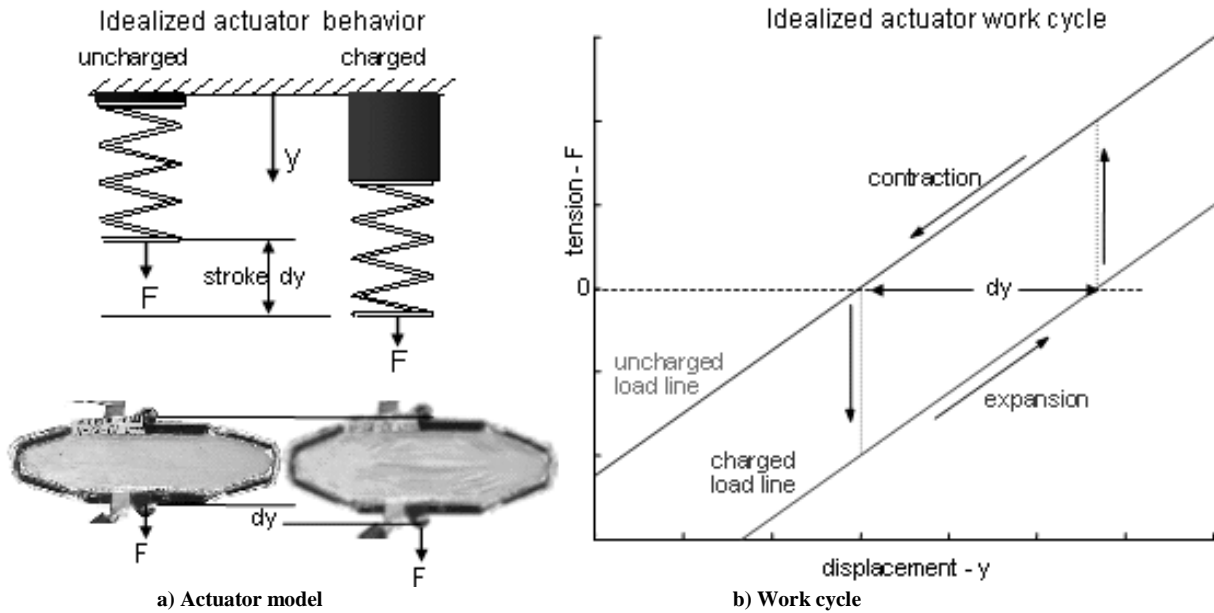


Figure 6. Idealized actuator model

In Figure 6b it can be seen that the vertical separation between the charged and uncharged stiffness curves represents the force differential the actuator can achieve if rigidly constrained. The horizontal separation of the curves at a given force corresponds to the actuator stroke, which is independent of external loading, provided the load remains constant throughout the stroke. Due to the compliance of the actuator, its length changes with external loading. The force generated by the actuator is not constant throughout the stroke. The force reaches its maximum at the beginning and linearly decreases to zero at the end of the stroke. However, for most applications including the BRAID, an actuator that provides uniform force is more desirable. Such actuator performance can be achieved by tuning the force displacement profiles in Figure 6b with a passive element.

3.4 Linear Bi-stable Elements

Figure 7 shows a linear bi-stable element (LBE) and its corresponding force-displacement characteristics. The LBE consists of a base that elastically supports two opposing flexure arms. As a slightly oversized insert is placed between the arms, it pre-loads the base and causes the assembly to have two stable configurations. Between these bi-stable states, there is a region where the force-displacement curve is approximately linear and has a negative slope, as shown in Figure 7b. The slope is a function of the geometry and material of the LBE. By varying the width of the insert, the slope of the force-displacement curve in the near-linear region can be tuned precisely. The stiffness of the actuator and LBE in parallel is equivalent to the sum of the actuator stiffness and LBE stiffness. Thus, by designing a LBE with a slope of negative 0.5N/mm over its linear range, the combined actuator module can be tuned to have zero stiffness (constant force output) over an operating range.

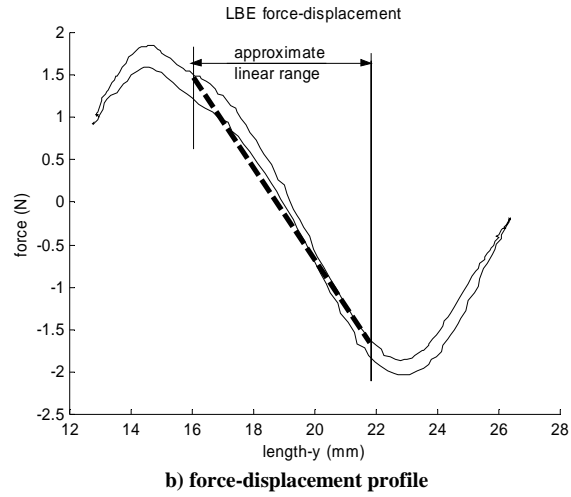
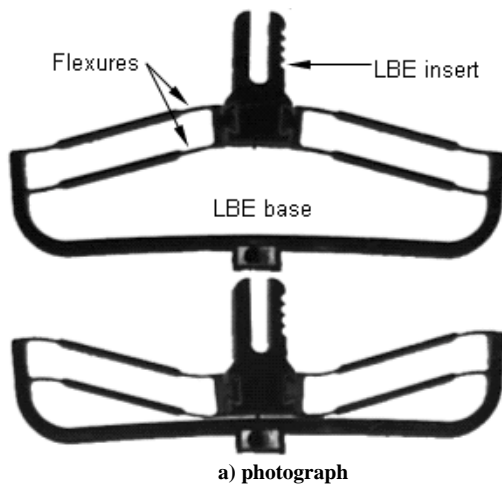


Figure 7. Linear bi-stable element

Figure 8a shows the force displacement characteristics of the combined actuator module including the passive element. The work cycle measurements presented Figure 5 were repeated. Figure 8a shows a range over which the actuator force is approximately constant. Comparing the work cycles in Figure 5 and Figure 8, the advantages of the compensated actuator become evident. The stroke of the actuator is increased from about 4mm to 8mm.

By using mechanical stops the actuator motion can be confined to the zero-stiffness range. Such an actuator has uniform force-displacement characteristics and reaches the same endpoints regardless of loading, provided it is within actuator capability. Thus such an actuator module provides robust binary operation. By using the actuator in a binary fashion, the hysteresis introduced by the viscoelastic properties of the elastomer is no longer a concern.

Figure 8b shows the displacement and current of the actuator versus time. Most of the current is drawn as the actuator charges. Some leakage current is drawn once the actuated state is reached. If the dielectric polymer actuator behaved as a true capacitor, there would be no current drawn at steady state. The actuator is switched off by draining the charge through a resistor. Theoretically, this energy could be recovered by circuitry and returned to an energy storage device such as a battery. While the voltage required for actuation is very high (5.5kV), the current drawn is extremely low. The peak current for the given actuator is about 0.03mA, which corresponds to a maximum electrical input of 0.165W.

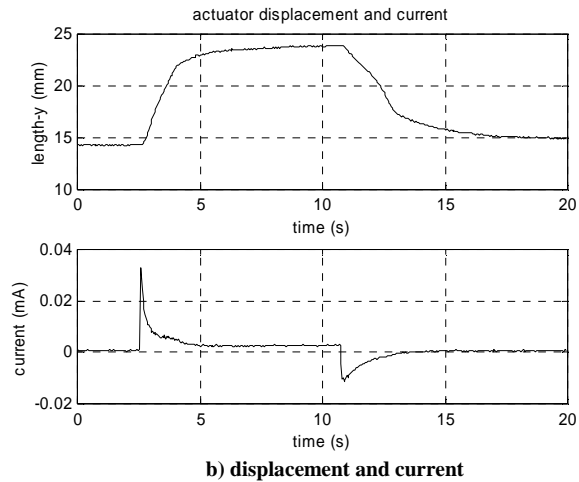
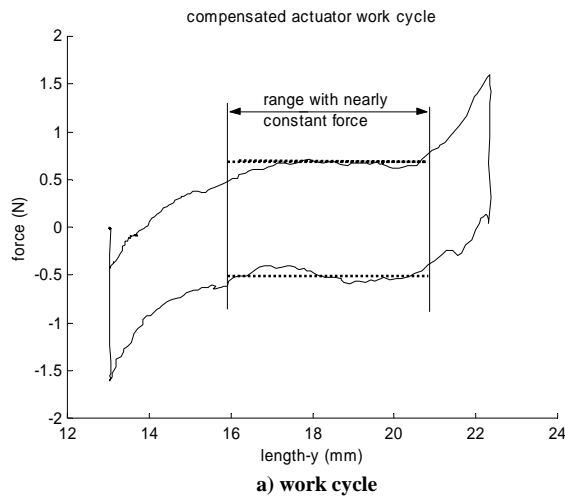


Figure 8. Performance of compensated actuator module

Figure 9 shows the actuator in its two states. The actuation force is about 1.5N. The actuator stroke is about 8mm, with the polymer film undergoing a strain of about 57%. The mass of a complete actuator unit is approximately 6 grams.

Most of this mass is due to the frame and bi-stable element. For a double-layered actuator, the mass of the dielectric polymer and electrodes itself is less than 0.1 grams, only a fraction of what the actuator is capable of lifting.

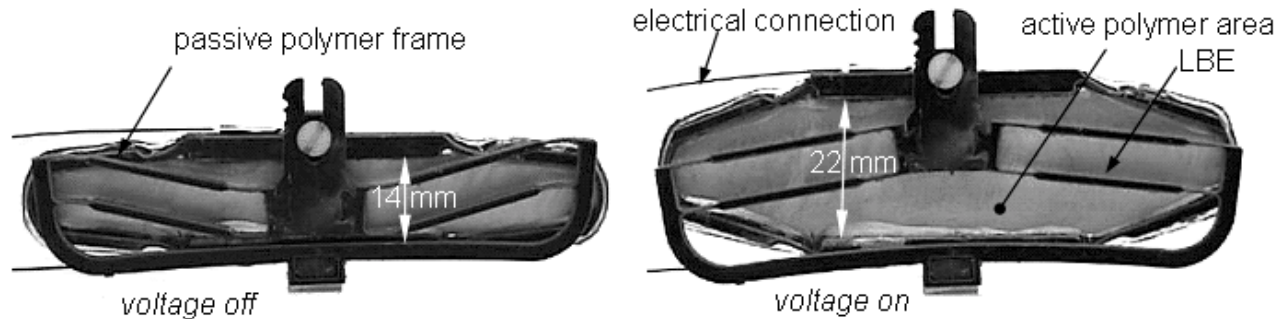


Figure 9. Embedded flexible-frame actuator

The range of motion of the actuator could be further increased by developing passive elements that have the desired negative stiffness over a larger range. The stroke of the current prototype is limited by the range of the LBE, rather than by the film or frame.

4 BRAID PROTOTYPE

When the actuators are implemented into the BRAID, they behave as structural elements with embedded actuation. Three parallel actuators form a single stage. A combination of identical stages forms the BRAID. The design goal of the BRAID is to produce a virtually all-plastic, lightweight, binary manipulator.

Figure 10 shows a photograph of a single BRAID stage before the dielectric polymer actuators are integrated. The kinematics of the mechanism requires a revolute joint at the bottom of the actuator and a spherical joint at the top. One rotational DOF is provided by a cross-flexural hinge machined from Delrin®. The hinge at the top of the frame approximates a spherical joint for small motions. It consists of thin compliant leaf that connects two pointed stiff elements.

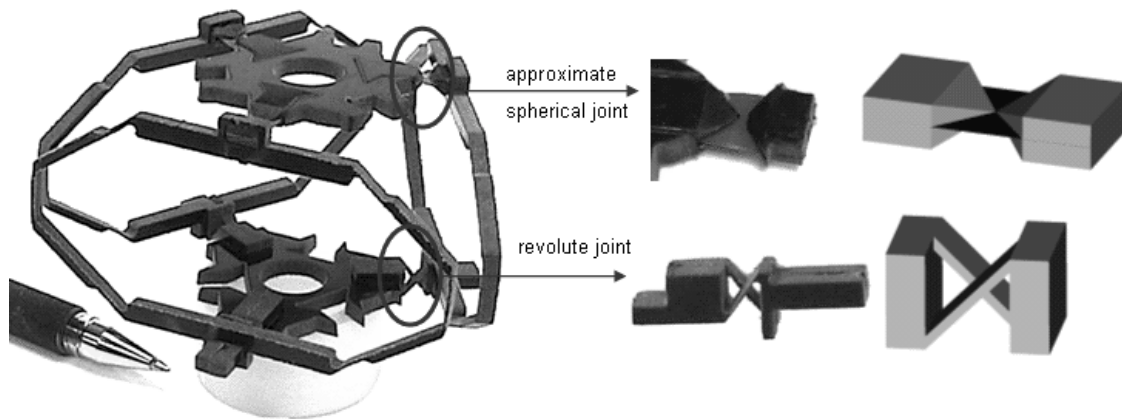


Figure 10. BRAID-skeleton without actuators

Figure 11 shows a 2-stage BRAID prototype manipulating a mirror. It has 6 binary DOF, allowing $2^6=64$ discrete states. Each degree of freedom is controlled by a simple switch. The total mass of the 2 stage BRAID prototype is about 65grams. The mass of the active actuator material itself, i.e. the dielectric film and electrodes, accounts for only 1% of the total mass. This suggests that most of the weight savings could be achieved by optimizing the structure rather than the actuators themselves.

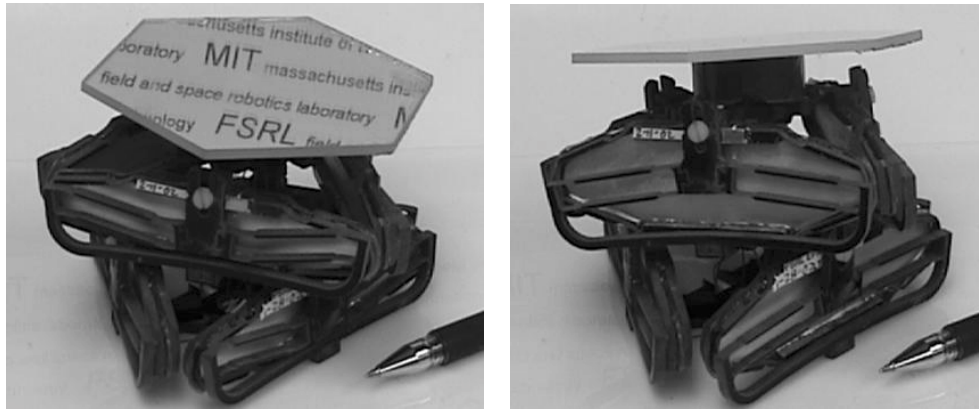


Figure 11. Photograph of a two-stage BRAID prototype

The performance of the BRAID presented here is sufficient to manipulate a small camera.

5 CONCLUSIONS

Dielectric polymer artificial muscles have been introduced to the field of high-DOF binary robotics. The performance of these actuators shows promise of making high-DOF binary robotic systems practical. The current challenge with dielectric polymer actuators lies with effectively implementing them such that their full potential is exploited to perform mechanical work. Here, this challenge was addressed by embedding the polymer actuators into flexible frames which maintained the desired boundary conditions on the actuator film. By adding a passive element, a self-contained actuator module was formed that could work both under tension and compression and produced approximately uniform force throughout the stroke. The active actuator area achieves a relative strain of 57% and provides a force of 1.5N, while weighing 6 grams. The 2-stage BRAID prototype shows promise that these actuators are a feasible alternative to conventional technologies in the near future. The simplicity of the actuators allows for a BRAID design that is virtually all-plastic, inexpensive, lightweight, and easy to control. Research in this program is continuing to develop devices that fully exploit the dielectric polymer actuators in very high DOF practical binary systems.

6 ACKNOWLEDGEMENTS

The support of the NASA Institute for Advanced Concepts (NIAC) for this research is acknowledged. The authors would like to thank Peter Weiss and Ebraheem Fontaine for their help in actuator development and fabrication of prototypes.

7 REFERENCES

- 1 G. Chirikjian, "A Binary Paradigm for Robotic Manipulators," *Proc. of IEEE International Conference on Robotics and Automation*, **Vol. 4**, pp. 3063-3069, 1994.
- 2 D. Lees, G. Chirikjian, "A Combinatorial Approach to Trajectory Planning for Binary Manipulators," *Proc. of the IEEE International Conf. on Robotics and Automation*, Minneapolis, MN, 1996.
- 3 M. Lichter, V. Sujun, S. Dubowsky, "Computational Issues in the Planning and Kinematics of Binary Robots," *2002 IEEE International Conference on Robotics and Automation*, Washington D.C., 2002.
- 4 M. Hafez, M. Lichter, S. Dubowsky, "Optimized Binary Modular Reconfigurable Robotic Devices," *2002 IEEE International Conference on Robotics and Automation*, Washington, D.C., May 11-15, 2002.
- 5 R. Pelrine, P. Sommer-Larsen, R. Konrbluh, R. Heydt, G. Kofod, Q. Pei, P. Gravesen, "Applications of Dielectric Elastomer Actuators," in *Smart Structures and Materials 2001: Electroactive Polymer Actuators and Devices*, Yoseph Bar-Cohen, Editor, Proceedings of SPIE **Vol. 4329**, March 2001.
- 6 K. Maejor, M. Rosenthal, R. Full, "Muscle-like actuators? A comparison between three electroactive polymers," *Smart Structures and Materials 2001: Electroactive Polymer Actuators and Devices*, Yoseph Bar-Cohen, Editor, Proceedings of SPIE **Vol. 4329**, pp. 7-15, March 2001.

- 7 V. Sujan, M. Lichter, S. Dubowsky, "Lightweight Hyper-redundant Binary Elements for Planetary Exploration Robots," *Proc. 2001 IEEE/ASME International Conference on Advanced Intelligent Mechatronics (AIM '01)* **811**, Como, Italy, July 2001.
- 8 R. Kornbluh, R. Pelrine, J. Joseph, R. Heydt, Q. Pei, S. Chiba, "High-field electrostriction of elastomeric polymer dielectrics for actuation," in *Smart Structures and Materials 1999: Electroactive Polymer Actuators and Devices*, Yoseph Bar-Cohen, Editor, Proceedings of SPIE **Vol. 3669**, pp. 149-161, 1999.
- 9 R. Pelrine, R. Kornbluh, Q. Pei, J. Joseph, "High Speed Electrically Actuated Elastomers with Strain Greater Than 100%," *Science*, **Vol. 287**, pp. 836-839, 2000.
- 10 R. Pelrine, R. Kornbluh, J. Eckerle, P. Jeuck, S. Oh, Q. Pei, S. Stanford, "Dielectric Elastomers: Generator Mode Fundamentals and Applications," in *Smart Structures and Materials 2001: Electroactive Polymer Actuators and Devices*, Yoseph Bar-Cohen, Editor, Proceedings of SPIE **Vol. 4329**, pp.148-156, March 2001.
- 11 S. Cho, S. Ryew, J. Jeon, H. Kim, J. Nam, H. Choi, and K. Tanie, "Electrostrictive Polymer Actuator Using Elastic Restoring Force," *Proceedings of 1st Intelligent Microsystem Symposium*, pp. 1963-1968, 2001.
- 12 J. Eckerle, S. Stanford, J. Marlow, J. Marlow, R. Schmidt, S. Oh, T. Low, S. Shastri "A Biologically Inspired hexapedal Robot Using Field-Effect Electroactive Elastomer Artificial Muscles," in *Smart Structures and Materials 2001: Electroactive Polymer Actuators and Devices*, Yoseph Bar-Cohen, Editor, Proceedings of SPIE **Vol. 4329**, March 2001.
- 13 R. Pelrine, R. Kornbluh, J. Joseph, "Electrostriction of polymer dielectrics with compliant electrodes as a means of actuations," *Sensor and Actuators A: Physical* **64**, pp. 77-85.
- 14 G. Kofod, R. Kornbluh, R. Pelrine, P. Sommer-Larsen, "Actuation response of polyacrylate dielectric elastomers," in *Smart Structures and Materials 2001: Electroactive Polymer Actuators and Devices*, Yoseph Bar-Cohen, Editor, Proceedings of SPIE **Vol. 4329**, p141-147, March 2001.

ON THE KINEMATICS OF PARALLEL MECHANISMS WITH BI-STABLE POLYMER ACTUATORS

Andreas Wingert,

Department of Mechanical Engineering

Massachusetts Institute of Technology, Cambridge, MA 02139 USA

arw@mit.edu

Matthew D. Lichter,

Department of Mechanical Engineering

Massachusetts Institute of Technology Cambridge, MA 02139 USA

lichter@mit.edu

Steven Dubowsky

Department of Mechanical Engineering

Massachusetts Institute of Technology Cambridge, MA 02139 USA

dubowsky@mit.edu

Abstract Binary robotic devices have been proposed to perform complex tasks. These systems do not require feedback and are very easy to control. Their kinematic performance approaches that of continuous devices as their degrees of freedom becomes large. To date, high DOF binary systems have not been demonstrated, largely due to actuator limitations. Recently, significant advances have been made with dielectric polymer actuators. Here it is shown that such actuators have the potential to make binary robotic devices practical. Two designs of a Binary Robotic Articulated Intelligent Device (BRAID) using dielectric polymer actuators are presented. The kinematic performance based on laboratory results and analysis is predicted.

Keywords: Parallel Mechanism, Binary, Bi-Stable, Dielectric Polymer Actuators, Double-Octahedral Variable Geometry Truss, BRAID

1 Introduction

Proposed future tasks for robotic systems such as for missions to Mars will require robot subsystems that are lightweight, inexpensive, and easy to control (Weisbin et al., 1999, Sujan et al., 2001). Conventional robotic technology does not meet these requirements. A key limitation is actuator performance. Recently, important progress has been made in

two areas that have the potential to meet this challenge. The first is hyper redundant binary robotic devices, and the second is dielectric polymer actuators (Pelrine et al., 2001). Here these two technologies are brought together in a concept called BRAID – Binary Robotic Articulated Intelligent Device. The BRAID is a lightweight, hyper-redundant binary manipulator with a large number of embedded actuators (Sujan et al. 2001). The kinematic performance is predicted based on measured results of actuator prototypes. Performance is also shown for projected performance of these actuators. Analysis suggests that dielectric polymer actuators have the potential of overcoming current actuator limitations and serving as a key component for high degree of freedom binary element manipulators. Such systems have the potential to be important in future robotic systems

2 Background and Literature

In the 1960's and 70's the concept of binary and sensorless robotics was introduced (Anderson et al., 1967, Roth et al., 1973). More recently increased computation power made the analysis, control, and planning for binary robots feasible (Chirikjian, 1994, Lees et al., 1996). Some experimental work has been done on binary redundant manipulators (Chirikjian, 1994). An example is a large variable geometry truss (VGT) manipulator that was constructed using pneumatic actuators. This implementation, while acceptable for systems with few DOF, cannot readily be extended to develop practical systems with very large DOF. To date, little work has been done to develop simple, lightweight, robust binary design concepts.

Development of dielectric polymer actuators started in the late 1990s (Pelrine et al., 1997). These actuators are one of a large class of electro active polymers (EAP) that has been studied (Madden et al., 2000). Recent progress has resulted from the identification of new and more effective dielectric materials, making it one of the most promising new actuator technologies, with relative strains of up to 380% having been reported (Pelrine et al., 2000, Pelrine et al., 2001). Applications such as robots, acoustic speakers, and solid-state optical devices have been proposed, including a snake-like manipulator using a small number antagonistic pairs of dielectric polymers, controlled in a conventional analog fashion (Pelrine et al., 2001).

To date, very high DOF binary robotic systems implemented with polymer actuators have yet to be explored. This is the subject of this paper. The focus is on the expected system kinematic performance given the demonstrated and anticipated actuator performances.

3 The BRAID

Figure 1 shows the kinematics for two designs of 3 degree-of-freedom parallel platforms. The first one is a revolute-revolute- spherical (RRS) configuration. The second one is a double-octahedral variable geometry truss (DOVGT) with a revolute-spherical-revolute (RSR) configuration (Rhodes et al., 1985). Each degree of freedom is binary-actuated, allowing a single stage to reach $2^3=8$ discrete states. The combination of identical stages forms the BRAID.

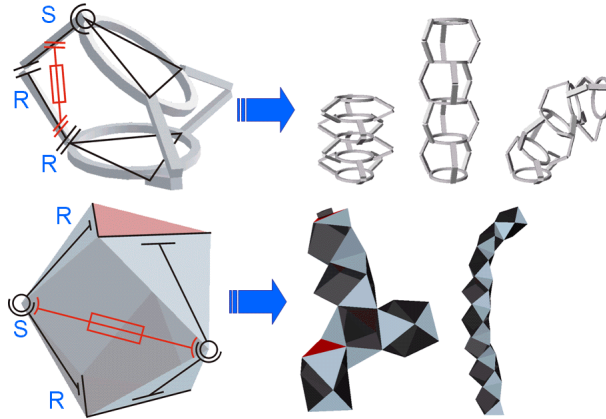


Figure 1 BRAID kinematics; top) RRS; bottom) RSR

As the number of stages of the BRAID increases, its performance approaches that of a continuous system (Lichter et al., 2002). The major advantage over conventional systems is that due to the on/off nature of each actuator and the two-state latching no feedback is required, which greatly simplifies control. The device also has good disturbance rejection and graceful failure modes. Figure 2 shows potential applications for space exploration of a 7-stage BRAID, such as a manipulator and a 6-legged walking rover.

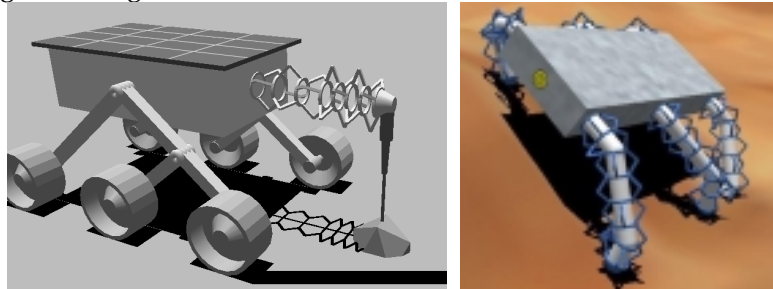


Figure 2 Application of the BRAID as a manipulator and as limbs of a walking robot

Implementing such systems as the BRAID with conventional actuators is not practical (Lichter et al., 2000, Chirikjian, 1994).

A first generation BRAID was built that used electromagnetic actuators (Hafez et al., 2002). It was found that the low force to weight ratio of the electromagnets greatly limited the number of stages, and hence the number of DOF. It is shown that dielectric polymer actuators have potential to be effective for this application. Figure 3 shows a sketch of how these actuators can be used into an RRS-BRAID.

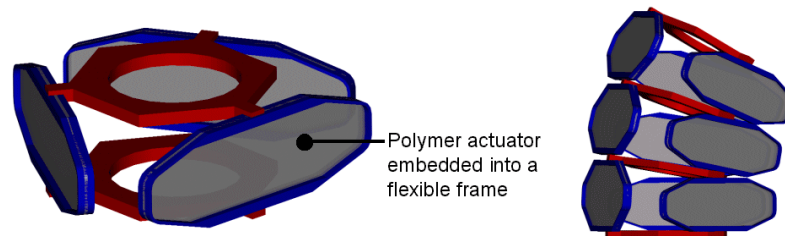


Figure 3 Polymer-actuated BRAID

4 Actuator Design

4.1 Dielectric polymer actuators

The operating principle of the dielectric polymer actuators is simple. An elastomeric film is coated on both sides with compliant electrodes. As a voltage is applied across the electrodes, the electrostatic charges will force the film to compress in thickness and expand in area (Peltine et al., 1997). This expansion in area can be used to actuate mechanical systems.

4.2 Actuator implementation

For most elastomeric film materials, the response is much larger if the film is pre-stretched in both planar directions (Kofod et al., 2001). For application in the BRAID, the film is placed between two flexible frames, which have a degree of freedom in the intended direction of motion. The frame ensures the desired boundary conditions on the film. It further supplies a restoring force to the stretched film, forming an actuator that can work under both tension and compression. The restoring force is also tuned by a passive bi-stable element, which effectively cancels the stiffness of the film and frame over a certain range. This increases the range of motion and ensures a nearly constant force throughout the actuator stroke. Figure 4 shows an actuator assembly before and after actuation. The relative strain of the active film is about 50%. The

actuator assemblies serve both as actuator and structural components when integrated into the RRS-BRAID (Figure 3).

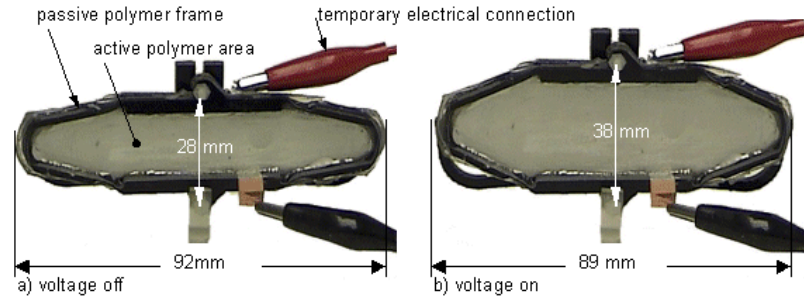


Figure 4 Photograph of embedded polymer actuator before and after actuation

4.3 Actuator Performance

The actuation forces are proportional to the cross sectional area of the film and can therefore be increased by combining multiple layers of the actuator material. Since a single layer of stretched dielectric material is only about $50\mu\text{m}$ thick, adding additional layers increases the actuation forces without significantly changing the geometry of the actuator. For an actuator with the same geometry shown in Figure 4, the actuation force is about 0.75N per layer.

The mass of a complete actuator unit is approximately 8 grams. Most of this mass is due to the frame and bi-stable element. For a double-layer actuator, the mass of the dielectric polymer actuator itself is less than 0.1 grams, only a fraction of what the actuator is capable of lifting. The performance of the actuator material is also independent of scale. In contrast to voice-coil actuators, which have poor performance on small scales, these actuators lend themselves for miniaturization (Pelrine et al., 2001). This suggests that the proposed BRAID can find applications on the micro- scale.

The actuator requires high voltage (5kV), but only draws currents of about $50\mu\text{A}$, hence they can be powered by conventional miniature batteries. New thinner films will result in lower voltages.

5 BRAID Kinematics and Workspace

To illustrate the current and predicted capabilities of a dielectric polymer powered BRAID, a 4-stage (12 DOF) device is considered. The workspace is a function of the geometry of the individual stages as well as the strokes of the actuators.

Figure 5a shows the workspace cloud of an RRS-BRAID that can be achieved readily with actuator performance demonstrated in laboratory experiments (Figure 4) (Wingert et al., 2002). The actuator overall length changes from 28mm to 38mm.

The size of the workspace is on the order of a single stage of the BRAID. The high density of the workspace would make such a design suitable for a micro-positioning device where high resolution is required rather than a large range of motion.

Dielectric polymer actuators have shown strains that are much larger under laboratory conditions than in the self-contained modular frame design described above. This suggests that the dominant limitation to system performance is not the actuator material itself. Optimization studies currently being performed on the frame and passive elements suggest that actuator strokes that are double those cited above will be demonstrated shortly. Figure 5b shows the significantly larger workspace, using an actuator that expands from 28mm to 48mm. The workspace diameter would then be on the order of the stowed RRS-BRAID height. Such a system lends itself to a variety of applications, such as a camera placement device for planetary exploration, see Figure 2.

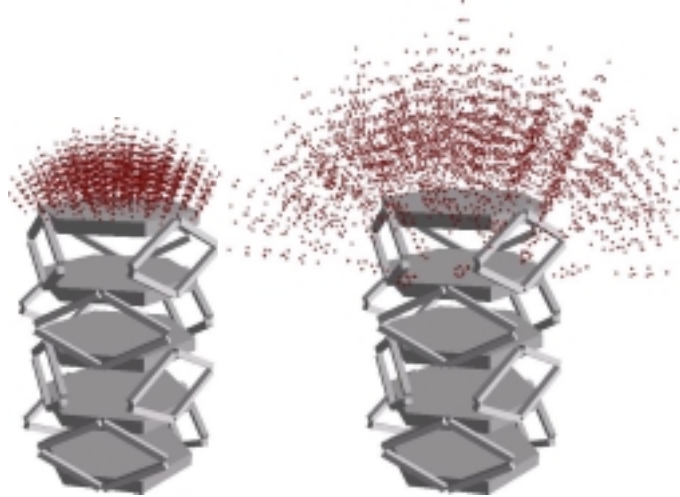


Figure 5 4-stage RRS-BRAID a) workspace with current actuator performance b) workspace with predicted actuator performance

A single stage of the RSR-BRAID has 14 faces, 8 of which have a fixed triangular geometry. The remaining 6 faces form diamond shapes that are occupied by dielectric polymer actuators (Figure 1). The RSR-stage is actuated by changing the diagonal lengths of the diamond-shaped areas

with the dielectric polymer. Actuators enclosed in a diamond-shaped frame have been successfully demonstrated.

One advantage of the RSR-BRAID over the RRS-BRAID is that the actuators are directly integrated into the structure, reducing the number of components. This comes at the cost of adding some complexity to the design process, as actuators and structure can no longer be tuned independently. The joints of the RSR-BRAID could be designed to provide the desired restoring forces. As with the previous design, the actuation forces can easily be increased by adding layers of actuator film.

Taking the currently achieved performance of the frame actuators and applying them to the RSR-BRAID results in a workspace shown in Figure 6a. If the effective motion of each actuator were to be doubled, a significantly larger workspace would be achieved (Figure 6b).

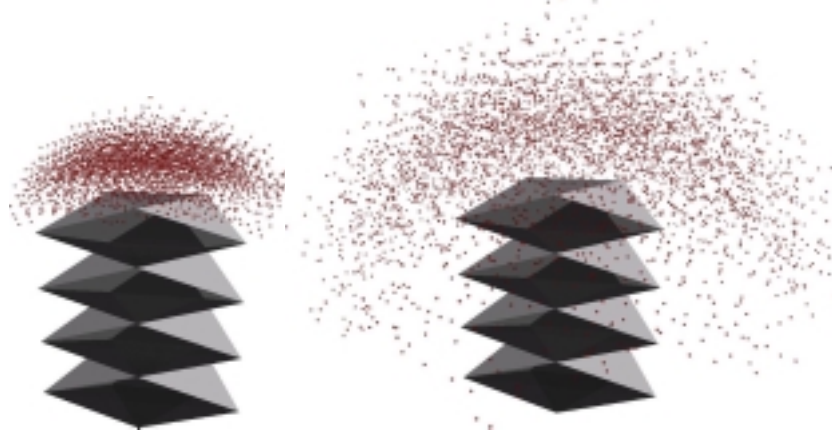


Figure 6 4-stage RSR - BRAID workspace cloud a) with current actuator performance b) with predicted actuator performance

6 Conclusion

It has been shown that dielectric polymer actuators have the potential of overcoming the key limitations of traditional actuators in making high-degree of freedom binary parallel robots practical. The simplicity of the actuators allows for a BRAID design that is virtually all-plastic, inexpensive, lightweight, and easy to control. Research in this program is continuing to develop devices that fully exploit the dielectric polymer actuators in very high DOF practical binary systems.

7 Acknowledgements

The support of the NASA Institute for Advanced Concepts (NIAC) for this research is acknowledged.

8 References

- Anderson, V., Horn, R. (1967) Tensor Arm Manipulator Design. *ASME paper*, 67-DE-57
- Chirikjian, G. (1994) A Binary Paradigm for Robotic Manipulators, *Proc. of IEEE International Conference on Robotics and Automation*, Vol. 4, pp. 3063-3069
- Hafez, M., Lichter, M., Dubowsky, S. (2002) Optimized Binary Modular Reconfigurable Robotic Devices, *IEEE International Conf. on Robotics and Automation*. Washington, D.C.
- Kofod, G., Kornbluh, R., Pelrine, R., Sommer-Larsen, P. (2001) Actuation response of polyacrylate dielectric elastomers, *Proc. of SPIE Vol. 4329*, pp. 141-147
- Lees D., Chirikjian, G. (1996) A Combinatorial Approach to Trajectory Planning for Binary Manipulators, *Proc. of the IEEE International Conf. on Robotics and Automation*, Minneapolis, Mn
- Lichter, M., Sujan, V., Dubowsky, S. (2000) Experimental Demonstrations for a New Paradigm in Space Robotics, *Proc. of the Seventh International Symposium on Experimental Robotics, ISER '00. Hawaii*, pp. 225-234.
- Lichter, M., Sujan, V., Dubowsky, S., (2002) Computational Issues in the Planning and Kinematics of Binary Robots, *ICRA*, Washington D.C.
- Madden, J., Cush, R., Kanigan, T., et al. (2000) Fast-contracting Polypyrrole Actuators, *Synthetic Metals*, 113: pp.185-193
- Pelrine, R., Kornbluh, R., Joseph, J., Chiba S., (1997) Electrostriction of Polymer Films for Microactuators, *Proc. IEEE Tenth Annual International Workshop on Micro Electro mechanical Systems*, Nagoya, Japan, pp. 238-243
- Pelrine, R., Kornbluh, R., Pei, Q., Joseph, J. (2000) High Speed Electrically Actuated Elastomers with Strain Greater Than 100%, *Science*, Vol. 287, pp. 836-839
- Pelrine, R., Sommer-Larsen, P., Kornbluh, R., Heydt, R., Kofod, G. Pei, P. Gravesen, Q. (2001) Applications of Dielectric Elastomer Actuators, *Proc. of SPIE Vol. 4329*
- Rhodes, M., Mikulas M., Jr., (1985) Deployable Controllable Geometry Truss Beam, *NASA Technical Memorandum*.
- Roth, B., Rastegar, J., Scheinman, V. (1973) On the Design of Computer Controlled Manipulators, *First CISM-IFTMM Symposium on Theory and Practice of Robots and Manipulators*, pp. 93-113
- Sujan, V., Lichter, M., Dubowsky, S., (2001) Lightweight Hyper-redundant Binary Elements for Planetary Exploration Robots, *Proc. IEEE/ASME Int. Conf. on Advanced Intelligent Mechatronics*, July 2001, Como, Italy.
- Weisbin, C., Rodriguez, G., Schenker, P., et al (1999) Autonomous Rover Technology for Mars Sample Return, *International Symposium on Artificial Intelligence, Robotics and Automation in Space (i-SAIRAS'99)*, 1-10.
- Wingert, A., Lichter, M., Hafez, M., Dubowsky, S. (2002) Plastic Hyper Redundant Robot Manipulators Actuated by Optimized Binary Electrostrictive Polymers, *SPIE Vol. 4695*, San Diego.